Earth Planet. Sci. Lett. 648 (2024) 119074

Contents lists available at ScienceDirect

Earth and Planetary Science Letters

journal homepage: www.elsevier.com/locate/epsl

Iron-sulfur-carbon redox interactions in the continental subduction factory and their effect on volatile element storage in the mantle wedge

Bibiana Förster [a], Sonja Aulbach [b,*], Gray E. Bebout [c], Gianluca Bianchini [d], Claudio Natali [e,f], Roberto Braga [a]

[a] Dipartimento di Scienze Biologiche, Geologiche ed Ambientali, Università di Bologna, Piazza di Porta San Donato 1, 40126 Bologna, Italy
[b] Institut für Geowissenschaften, Goethe-Universität Frankfurt, 60438 Frankfurt am Main, Germany
[c] Department of Earth and Environmental Sciences, Lehigh University, 1 West Packer Avenue, Bethlehem, PA 18015, USA
[d] Dipartimento di Fisica e Scienze della Terra, Università di Ferrara, Via Saragat 1, 44124 Ferrara, Italy
[e] Dipartimento di Scienze della Terra, Università degli studi di Firenze, Via Giorgio La Pira, 4, Firenze I-50121, Italy
[f] CNR - Istituto di Geologia Ambientale e Geoingegneria, Unità di Montelibretti, Area Territoriale di Ricerca di Roma 1, Strada Provinciale 35d, 9, Montelibretti (RM) I-00010, Italy

ARTICLE INFO

Keywords:
Volatile element cycle
Oxygen fugacity
Continental collision
Orogeny
Subcontinental lithospheric mantle
Stable isotopes

ABSTRACT

The ultramafic rocks of the Ulten Zone tectonic mélange experienced a well-documented multi-stage metamorphic history, from residence in a hot mantle wedge to down-dragging and trapping in a Variscan slab accompanied by amphibolitisation, and finally two-stage exhumation accompanied by chloritisation and serpentinisation. We use these rocks as a natural laboratory to investigate whether volatile element fluxes in continental subduction zones promote long-term volatile element storage in the overlying mantle wedge. Here, we obtained new data on the chemical composition, iron speciation, carbon concentrations and isotopic compositions of ultramafic bulk rocks, and the carbon-oxygen isotope composition of carbonates in samples from >10 ultramafic lenses, which we combine with previously published data for additional insights.

The carbonate stable isotope compositions show a distinct provinciality, whereby rocks from the little retrogressed ultramafic lenses in the NE Ulten Zone domain have lower average $\delta^{13}C_{V\text{-}PDB}$ and $\delta^{18}O_{V\text{-}SMOW}$ of –16.8‰ to –5.7‰ and +8.0‰ to +17.8‰, respectively, than those in the more retrogressed SW domain (–11.2‰ to 0.0‰ and +12.9‰ to +20.7‰, respectively), suggesting influx of distinct crustal fluids. Bulk-rock carbon contents range from 130 to 28,000 μg g^{-1}, exceeding estimates for the convecting mantle, and are on average higher in rocks from the NE domain (median 880 μg g^{-1}), which can be modelled as Rayleigh-style dolomite addition at ~800–700 °C. Rocks from the SW domain have lower C contents (median 570 μg g^{-1}) which correlate positively with $\delta^{13}C$ and can be modelled as Rayleigh-style calcite addition at ~500–400 °C. The lowest $\delta^{13}C$ and C contents point to dedolomitisation during low-temperature (400 °C) serpentinisation, and furthermore suggest the contribution of a ^{13}C-depleted phase to the bulk-rock compositions.

After melt depletion during formation of the pre-Variscan continental lithosphere, the sulfur inventory was replenished during amphibolitisation near peak-metamorphic conditions, via sulphidation during interaction with siliceous fluid. Sulfur was markedly (re-)depleted during processes related to exhumation, reflecting low sulfur fugacity during chloritisation and serpentinisation. The available data suggest that the high bulk-rock $Fe^{3+}/\Sigma Fe$ (median 0.18) resulted from reduction of some aqueous sulphate during amphibolitisation, accompanied by redox-neutral carbonation, and from carbonate reduction during chloritisation when sulfur fugacity was low.

Ignoring exhumation-related C loss and taking near-peak metamorphic conditions as representative, significant amounts of C in carbonates and water in amphiboles may be stored in continental mantle wedges. These are subsequently stabilised below collisional orogens, which cover vast areas of Earth's continents and possibly constitute particularly volatile element-rich lithospheric mantle reservoirs.

* Corresponding author.
E-mail address: s.aulbach@em.uni-frankfurt.de (S. Aulbach).

https://doi.org/10.1016/j.epsl.2024.119074
Received 8 April 2024; Received in revised form 10 October 2024; Accepted 12 October 2024
Available online 28 October 2024

1. Introduction

Volatile elements (e.g., C, S, H) are known to affect the rheology of the mantle and therefore large-scale processes, such as plate tectonics and lithospheric stability; they are critical to mobilising ore-forming metals; and they depress the mantle solidus, facilitating the generation of melts and the release of climate-active magmatic gases to the atmosphere (e.g., Bekaert et al., 2021; Gibson and McKenzie, 2023, and references therein). Their role in global geodynamics and mass cycles cannot be overemphasised, and identifying the main volatile element reservoirs and fluxes remains one of the most important challenges in geosciences. The consumption of ocean basins during the convergence of continental plates eventually leads to burial of a continental slab and collision, effectively ending convergence (Zheng and Chen, 2016). Before the lithosphere stabilises, continental collision zones are sites of crust-mantle interactions that may eventually lead to the long-term storage of volatile elements in the overlying continental lithospheric mantle. The underappreciated role of the lithospheric mantle as a transient reservoir, which may capture volatile elements during metasomatic interaction with fluids (aqueous fluid, supercritical liquid or melt) and release them during subsequent tectonic perturbations, has been highlighted in recent studies (Gibson et al., 2020; Gibson and McKenzie, 2023). The importance of continental lithospheric mantle in global volatile element cycles derives also from its longevity, providing ample time for metasomatic overprinting (e.g., Aulbach, 2019). Lithospheric mantle stabilises by partial melt extraction, during which most volatile elements behave incompatibly, leaving a residue that is volatile element-depleted. Trace quantities of volatile elements that were not consumed during partial melting are stored in nominally volatile-free minerals and/or in volatile-bearing minor and trace phases (e.g., hydrous minerals, sulphide minerals, metal, graphite/diamond or carbonate) that may be metasomatically added under appropriate pressure (P), temperature (T) and oxygen fugacity (fO_2) conditions (e.g., Peslier, 2010; Stagno et al., 2019; O'Neill, 2021).

Despite a plethora of observations from field and experimental studies, and recent advances in thermodynamic modelling, the source and medium for re-introduction of volatile elements into this refractory lithospheric mantle residue, and the attendant redox interactions, remain to be unravelled. Interaction with subduction-derived fluids is one of the main vectors by which lithospheric mantle is re-enriched in volatile elements (e.g. Scambelluri et al., 2016; Foley and Fischer, 2017; Gibson and McKenzie, 2023). However, current box models reveal an extreme degree of uncertainty regarding the role of the continental mantle as a volatile element reservoir. As an example, estimates of C flux into the lithosphere range from zero to 47 Mt yr^{-1} (Kelemen and Manning, 2015). The locus, speciation and extent to which S is liberated from the slab are similarly uncertain, as thermodynamic modelling and the message from natural samples produce conflicting results, and the involvement of oxidised S in the observed oxidation of the mantle wedge and arc magmas remain hotly debated (e.g., Cottrell et al., 2022; Evans et al., 2022). Part of the uncertainty on the recycling efficiency of volatile elements stems from its dependence on intensive parameters (e.g., P, T and fO_2). These parameters determine the mineralogy of the down-going slab and the speciation of C and S, the solubility and mobility of which (in fluids) increase drastically when oxidised (e.g., Frezzotti et al., 2011; Tomkins and Evans, 2015).

Based on evidence for the (redox) interactions between Fe, C and S in subduction-modified mantle rocks (e.g., Debret et al., 2014, 2020; Rielli et al., 2017, 2018), it is clear that these multi-valent elements must be considered in concert in order to understand the mobility and sequestration of volatile elements in subduction zones. Here, we study peridotites and pyroxenites from the Ulten Zone tectonic mélange, which experienced a well-constrained metamorphic evolution. Previous work established that multiple episodes of crust-mantle interaction led to addition of hydrous minerals, carbonates and sulphides, involving crustal melts near peak-metamorphic conditions and crustal COH fluids during subsequent exhumation (Godard et al., 1996; Hauzenberger et al., 1996; Martin et al., 1998; Rampone and Morten, 2001; Tumiati et al., 2003; Marocchi et al., 2009; also see next section, Text S1 and Fig. 1). Accordingly, Consuma et al. (2021) successfully modelled the Sr-S isotope compositions of Ulten Zone clinopyroxene/amphibole and sulphide, respectively, as the result of mixing of depleted mantle with a crustal component having high-$\delta^{34}S$ – high-$^{87}Sr/^{86}Sr$. The aim of this study is to constrain the nature and variability of redox interactions in continental subduction zones that led to precipitation or removal of carbonate and sulphide minerals. For this, we acquired new bulk-rock C concentrations and isotope compositions as well as Fe speciation data, combined with C and O isotope composition of the carbonate minerals contained therein.

2. Geology, prior work and samples

The Ulten Zone is a tectonometamorphic complex in the Italian Alps (Fig. 1a) that experienced Variscan continental collision but only weak Alpine overprinting (Godard et al., 1996). Extensive prior work presented in detail in Text S1 has paved the way for the present study and only a brief summary is provided here. In the Ulten Zone, peridotite lenses, which likely originated as continental lithospheric mantle, occur within a lower unit of garnet- and kyanite-bearing gneisses and an upper unit of migmatitic gneisses (Godard et al., 1996) (Fig. 1a). Geochronological constraints summarised in Tumiati et al. (2003) suggest a pre-Variscan protolith that became the hanging wall of a Variscan continental subduction zone (Godard et al., 1996; Hauzenberger et al., 1996; Martin et al., 1998).

A four-stage metamorphic evolution during Variscan collision and post-collisional exhumation is recognised, for which conventional geothermobarometry, consideration of phase stabilities and geodynamic modelling have allowed P-T estimates to be made (Nimis and Morten, 2000). Complementary geochronological study (Tumiati et al., 2003, and references therein) and numerical modelling constraints (Ranalli et al., 2005) provide a timeline (Fig. 1b). The attendant mineralogical changes, which are also visible in the pyroxenites thought to have originated by interaction with or precipitation from mafic melts in the hot mantle wedge (Gudelius et al., 2019, references therein), are summarised in Fig. 1c. The Mt. Hochwart locality (Fig. 1a) represents the direct contact between the peridotite lenses and the crustal gneisses (Marocchi et al., 2009). Oxygen fugacity estimates (relative to the Fayalite-Magnetite-Quartz buffer FMQ) for Ulten Zone garnet peridotites vary widely, from FMQ-2.4 to FMQ+2 (Fig. 1d), and show no relationship with textural type (Malaspina et al., 2009; Gudelius et al., 2019). The latter work also revealed a marked provinciality in the NE and central Ulten Zone domains with respect to chemical and isotopic composition (more details in Text S1).

In addition to a legacy collection at Università di Bologna, new samples were collected during more recent field campaigns (Förster et al., 2017; Gudelius et al., 2019) (Table S1), significantly extending the number of studied ultramafic lenses from the Ulten Zone tectonic mélange. Combined, they form the basis of the present study, for which samples were selected that are representative of the various petrographic peridotite types (Table S2). They are therefore considered representative of the different evolutionary stages in pressure-temperature space shown in Fig. 1b and mineral assemblages shown in Fig. 1c. The samples contain multiple generations of carbonate minerals (Fig. 1c), examples of which are shown in Fig. 2.

3. Sample preparation and analytical techniques

3.1. Sample preparation

For the production of bulk-rock powder, hand specimens of selected samples were cut into cm-sized blocks representative of an unweathered mineral composition of the rock, exclusive of veins. Bulk-rock powders

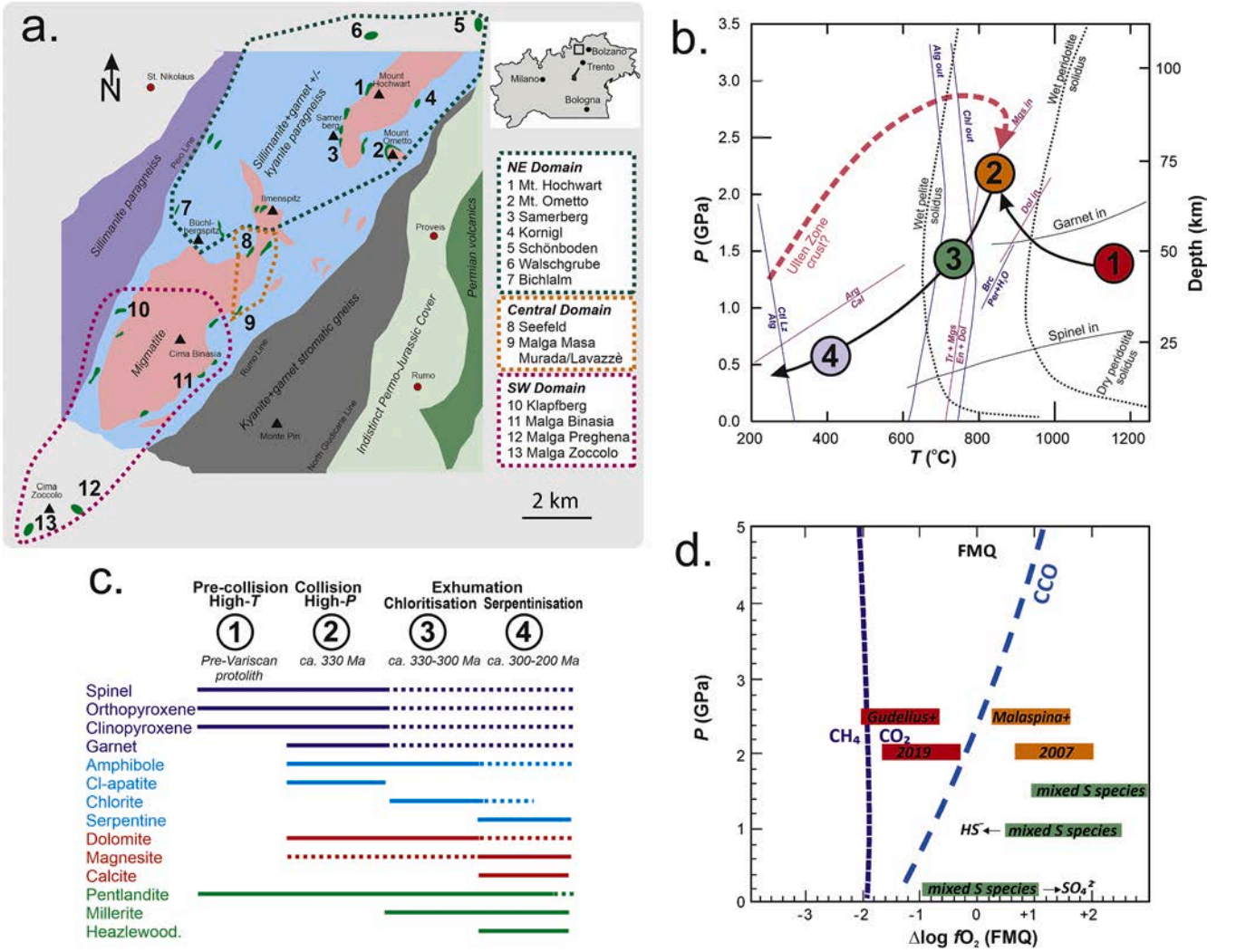

Fig. 1. Geological background and metamorphic evolution of the Ulten Zone tectonic mélange. a. Map showing various peridotite lenses (green; displayed somewhat larger than in the field for visibility; for orientation, lens 5 is at 46°31′45″, 11°02′13″, and lens 13 at 46°24′38″, 10°52′47″) concentrated at the contact between migmatites and paragneisses, adjacent geological units, prominent alpine peaks (black triangles) and towns (red circles) in the Ulten Zone (based on Förster et al., 2017 and Consuma et al., 2021, references therein). The assignment of individual localities to lenses is approximate. Three domains are recognised based on geochemical and isotopic characteristics (Gudelius et al., 2019, 2022; this work). b. *P-T* diagram illustrating the 4-stage metamorphic evolution of Ulten Zone peridotites. Also shown are relevant phase relations for hydrous minerals (Ctl crysotile, Lz lizardite, Atg antigorite, Chl chlorite, Brc brucite, Hbl horndblende, Tr tremolite) and carbonate minerals (Arg aragonite, Dol dolomite, Cal calcite, Mgs magnesite), and wet and dry solidi (also: En enstatite, Per periclase, Grt garnet, Spl spinel) (based on Consuma et al., 2021, references therein, complemented by a possible crustal path in Gudelius et al., 2019, references therein). The timing of entrapment in the crust – during or shortly after the high-pressure stage – is controversial (Tumiati et al., 2003; Scambelluri et al., 2006). c. Summary of rock-forming and accessory volatile-bearing minerals related to the 4 metamorphic stages of Ulten Zone peridotites (based on Consuma et al., 2021). The associated timeline is from Tumiati et al. (2013) and Ranalli et al. (2005). d. $\Delta\log fO_2$(FMQ) vs. *P*, showing speciation for CHO fluids and the CCO oxygen buffer ($C + O_2 = CO_2$) (references in Consuma et al., 2021). Valence state transition of sulfur in basaltic to andesitic melts for various pressures at 850–1050 °C is from Matjuschkin et al. (2016) who note that bulk compositional effects, while non-negligible, are smaller than *P* effects; the green bars depict the fO_2 range where mixed valence is expected, almost all sulfur would be reduced to the left and oxidised to the right. Distinct results (using the same oxybarometer and method to determine garnet Fe^{3+}) for Ulten Zone garnet peridotites obtained by Malaspina et al. (2009) and Gudelius et al. (2019) are shown for two plausible pressures, illustrating the fO_2 variability of subduction-modified peridotite even in a single tectonic mélange.

were obtained by crushing the blocks into granulate using a mechanical rock crusher and by grinding the granulate using a vibratory agate disc mill.

3.2. Determination of bulk-rock major-/trace element compositions and iron speciation

Twenty-two representative samples (5 coarse-grained protogranular-porphyroclastic spinel peridotites, 1 coarse-grained peridotite with coronitic garnet, 9 fine-grained garnet-amphibole peridotites, 7 fine-grained garnet-free spinel-amphibole peridotites) were chosen for bulk-rock geochemical characterisation (Table S2). Analyses of bulk-rock major and trace elements were performed at Activation Laboratories (Ontario, Canada; www.actlabs.com; see website for detailed information of analytical techniques and detection limits) with the analytical package "4Lithores" using a Perkin Elmer Sciex ELAN 6000/6100/9000. Whole-rock major-element compositions were analysed by ICP-AES (inductively-coupled plasma atomic emission spectroscopy). After cold acid digestion with ammonium metavadanite and hydrofluoric acid, concentrations of FeO were determined by potassium dichromate back-titration of the reduced V, allowing to estimate bulk-rock Fe_2O_3 concentration and $Fe^{3+}/\Sigma Fe$ from $Fe_2O_3^{total}$, with estimated

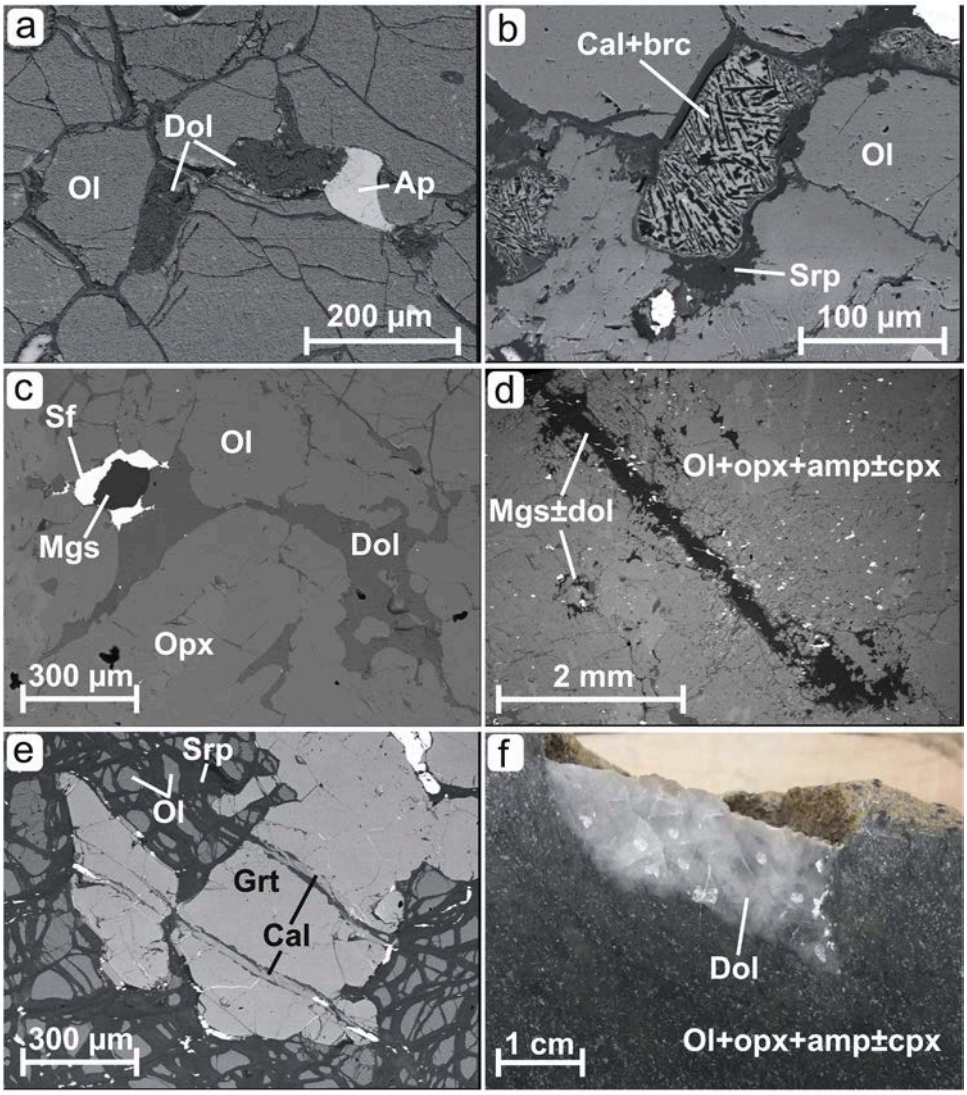

Fig. 2. (a–e) Back-scattered electron images showing (a) discrete dolomite grains in the matrix of little-serpentinised fine-grained garnet-amphibole peridotites associated with apatite (sample SBA7); (b) calcite-brucite symplectites (dedolomitization products: Förster et al., 2017), situated in the serpentine mesh texture of serpentinised fine-grained garnet-amphibole peridotite (sample WG2); (c) interstitial anhedral dolomite and magnesite with curvilinear contacts against matrix minerals; (d) a magnesite vein crosscutting the matrix of coarse-grained protogranular peridotite MOL1.5; (e) calcite veinlets related to magnetite situated in the serpentine mesh texture and crosscutting garnet (sample SB3.2, serpentinised fine-grained garnet-amphibole peridotite); (f) photograph of polycrystalline aggregate of dolomite (~5 cm length) in fine-grained garnet-amphibole peridotite VM25P11; the drill pits after micro-drilling for stable-isotope analyses are visible. Mineral abbreviations after Whitney & Evans (2010), sf: sulphide.

relative uncertainties of 5% (by reference to similar methods; Gudelius et al., 2019). Bulk-rock trace-element compositions were analysed by ICP-MS (inductively-coupled plasma-mass spectrometry). Results are reported in Table S3.

3.3. Determination of bulk-rock total carbon concentrations and carbon isotope compositions

Following initial semi-quantitative tests with a LECO RC-412 Multiphase Carbon Determinator to obtain C mass fractions released at 550 and 1000 °C (Text S1, Table S4), total elemental C concentrations and bulk-rock C isotopic ratios were obtained for 54 representative samples (12 coarse-type peridotites, 17 fine-grained garnet-bearing peridotites, 21 fine-grained garnet-free peridotites, 4 amphibolitised pyroxenite samples, in addition to 4 crustal samples; Text S1). These analyses were performed at the University of Ferrara (Italy) using a Continuous Flow Isoprime100 Isotope Mass Spectrometer coupled to a Micro Cube Elemental Analyzer (EA-CF-IRMS). The application of this technique to study the C concentration and C isotopic composition in low-C matrices such as peridotites, was described by Bianchini and Natali (2017). The reliability of the analytical results was tested as described in Text S1. The maximum variation of $\delta^{13}C$ ($\Delta^{13}C$) for duplicates is 0.54‰, which is smaller than the symbols in the $\delta^{13}C$ diagrams. Results, including petrographic type, are reported in Table S5. The elemental precision, estimated by repeated standard analyses, and accuracy, estimated by the comparison between reference and measured values, were on the order of 5% of the absolute measured value. The uncertainty increased for concentrations approaching the detection limit (0.01 wt. %).

3.4. Determination of carbonate carbon and oxygen isotope compositions

Preparation and analysis of the O and C isotopic compositions of bulk carbonate in peridotites, and of micro-drilled carbonates, were performed at Lehigh University (USA). Peridotite whole-rock powder was reacted with phosphoric acid at 72 °C resulting in the dissolution of the

carbonate minerals in the samples. Due to the low and highly variable modal abundance of carbonate minerals in the peridotites (based on petrographic observations), this was preceded by extensive tests. The aim was to determine the appropriate amount of bulk-rock powder required for carbonate dissolution to produce as much as CO_2 as needed to yield reliable intensities (>0.5 mV) (Text S1 and Figs. S2 and S3). In addition, carbonate minerals in different textural sites were sampled by micro-drilling (with a 1 or 2 mm diameter bit, depending on textures) and reacted with 0.2 ml phosphoric acid, with reaction times adjusted for complete CO_2 release accepted for pure calcite, pure dolomite and pure magnesite of $\geq$ 0.5, 3 and 30 h, respectively. Isotope ratios were measured using a Finnigan MAT 252 interfaced with a GasBench II system. Analyses of an in-house calcite standard and the international calcite standard NBS-19 were obtained to, respectively, monitor and correct the isotopic data, with a standard deviation (1σ) of $\leq$ 0.2‰ for both $\delta^{13}C$ and $\delta^{18}O$. The notations reflect ‰ deviations from Pee Dee Belemnite (V-PDB) and Standard Mean Ocean Water (V-SMOW), respectively. Results are reported in Table S6.

4. Results

4.1. Bulk-rock major element compositions

Bulk-rock Al_2O_3 and CaO concentrations range from 1.50 to 3.71 wt. % and 1.18–3.11 wt. %, respectively (Table S3). In general, major-element compositions are well within the range of previously reported compositions (Fig. S4). The LOI values, as a measure mostly of amphibole, chlorite and serpentine modal abundances, with subordinate contributions from carbonate-derived CO_2 (see C concentrations in Tables S4 and S5), range from 0.25 to 7.72 wt.-% and conform to the hydration degrees of the peridotites observed during petrographic investigation (i.e. modal abundance of amphibole, chlorite, serpentine).

4.2. Bulk-peridotite carbon concentrations and isotopic compositions

The total carbon concentration in Ulten Zone ultramafic rocks was measured in samples of different petrographic types, and ranges from 0.02 to 0.29 wt. % for measurements with the LECO multiphase carbon determinator (Table S4; $n = 51$), and from 0.01 to 0.28 wt. % for measurements with the Micro Cube Elemental Analyzer (Table S5; $n = 54$). The data agree well, with the majority of all samples (80%) containing total carbon in the range of 0.03 to 0.10 wt. % (Fig. S5).

$\delta^{13}C$ of the bulk-rock ultramafic rocks ranges from −21.5‰ to −6.7‰, the majority of which (72%) displaying $\delta^{13}C$ between −15‰ to −10‰ (Table S5). The concentration of total C and the $\delta^{13}C$ values do not show any correlation to the individual petrographic types of peridotite (Fig. S5). Exceptions are one coarse-grained garnet-bearing peridotite and the amphibolitised pyroxenite samples which exhibit very low total C concentrations and $\delta^{13}C$. For comparison, the crustal rocks' total C content (0.05 to 0.22 wt. %) is similar to that of the Ulten Zone peridotites, whereas the $\delta^{13}C$ is more negative (−33.0‰ to −25.4‰). The variabilities of the total C content and $\delta^{13}C$ in Ulten Zone ultramafic rocks are related to provenance: samples from SW localities in the Ulten Zone show strong variability of $\delta^{13}C$ (−21.0‰ to −6.7‰) and relatively low C contents (0.01 to 0.10 wt. %). Conversely, samples from the NE of the Ulten Zone exhibit a narrower range in $\delta^{13}C$ but increasing total C concentrations ($\delta^{13}C$ from −15.1‰ to −10.3‰, one exception −21.5‰, and from 0.03 to 0.28 wt. % total C). Among the latter, two samples containing magnesite veins display the highest concentrations (0.17 and 0.28 wt. %).

4.3. Carbon and oxygen isotopic compositions of carbonate minerals

Carbon and O isotope compositions of carbonate minerals in 128 Ulten Zone peridotite samples were determined for carbonate in whole-rocks and micro-drilled carbonate minerals (Table S6). The $\delta^{13}C$ of for carbonate in whole rocks ranges from −14.6‰ to 0.0‰ and $\delta^{18}O$ ranges from +9.9‰ to +20.7‰.

The $\delta^{13}C$ values of the micro-drilled dolomite aggregate from the fine-grained, garnet-bearing, slightly serpentinised sample VM25P11 (Fig. 2f) ($\delta^{13}C$ from −10.1‰ to −9.6‰) are similar to the $\delta^{13}C$ values of dolomite in similar rocks (samples SBA 4/5/7), whereas the $\delta^{18}O$ values of +6.4‰ to +10.4‰ are lower than those of all other samples; Table S6). The whole-rock carbonate $\delta^{13}C$ value in the slightly serpentinised coarse-grained, garnet-free sample MOL1.5 (−10.31‰) overlaps those of a micro-drilled dolomite grain ($\delta^{13}C$ of −10.1‰ and −9.4‰) and of a micro-drilled magnesite vein (−10.9‰ to −10.7‰) in the same sample. In contrast, the isotopic compositions of a micro-drilled magnesite vein in the serpentine-bearing, amphibole-rich sample KoD9 from the Kornigl locality ($\delta^{13}C$ of −16.8‰ to −13.8‰; $\delta^{18}O$ of +9.8‰ to +11.0‰) differ from those of the corresponding whole-rock carbonates ($\delta^{13}C$ −9.7‰, $\delta^{18}O$ +16.4‰).

Comparison of the C isotopic compositions of the whole-rock peridotites and the carbonate minerals contained therein shows that the whole-rock $\delta^{13}C$ values are generally more negative than the carbonates (Tables S5 and S6) for almost all samples.

5. Discussion

5.1. Carbonate mineralogy and isotopic composition linked to mantle wedge evolution

The well-constrained *P-T* (Fig. 1b) and mineralogical (Fig. 1c) evolution of the Ulten Zone peridotites, including the presence of different carbonate minerals in different textural settings, allows delineation of the response of $\delta^{13}C$ and $\delta^{18}O$ to these changes in *P-T* and mineralogy. Prior work (e.g., Marocchi et al., 2009; Sapienza et al., 2009; Malaspina and Tumiati, 2012; Förster et al., 2017; also Text S1) established that dolomite dominantly represents an early phase. According to these studies, dolomite was possibly precipitated already at the hot mantle wedge stage (dolomite inclusions in primary spinel from coarse peridotite). This dolomite appears to be in textural equilibrium with matrix minerals in garnet peridotites, together with amphibole and apatite, although secondary dolomite veins are also observed (see e.g. images in Sapienza et al., 2009; Förster et al., 2017; Consuma et al., 2020). Magnesite typically replaces dolomite (Stage 2; Fig. 1b) or occurs as texturally late-stage veins (Stage 4). It is often associated with retrograde minerals such as serpentine, whereas calcite veinlets are always associated with serpentinisation (stage 4), as are brucite and magnesite intergrowth after dolomite (Fig. 2b). The $^{87}Sr/^{86}Sr$ ratios for carbonate minerals in diverse textural positions show an evolution, with moderately elevated values (~0.705) for discrete matrix dolomite vs. highly radiogenic values (up to 0.7083) for vein dolomite (Consuma et al., 2020). Thus, the carbonate mineral evolution qualitatively suggests an increasing influx of crustal-derived fluid characterised by variable CO_2/H_2O (Rampone and Morten, 2001; Förster et al., 2017), but evolving to low $a(CO_2)$ during serpentinisation. The co-precipitation of amphibole and dolomite during Stage 2 is supported by the similarity of their $^{87}Sr/^{86}Sr$ (Consuma et al., 2021).

Amongst the studied samples, peridotites from the crust-mantle contact at Mount Hochwart may reflect the most intense interaction of crust-derived fluids or melts with the mantle, characterised by formation of metasomatic reaction bands, including zircon yielding a 333 Ma U-Pb age, identical to migmatisation of the crustal rocks (Tumiati et al., 2003, 2007). This caused the transfer of H_2O, K_2O and LILE from the crust and the formation of phlogopite, anthophyllite and talc at the crust-mantle interface (Marocchi et al., 2009). As the dolomites at Mount Hochwart have $\delta^{13}C$ around −10‰, and if the crust-mantle interaction at Mount Hochwart was mediated by a crustal fluid around 660–700 °C (Fig. 1b) (Tumiati et al., 2007; Marocchi et al., 2009), the $\delta^{13}C$ of the fluid would have been only ~0.6‰–0.8‰ lighter than dolomite, that is −10.6‰ to −10.8‰ (Text S1). The residual pre-Variscan lithospheric mantle, which

experienced extraction of 10–20% partial melt at minimum (Ionov et al., 2017; Gudelius et al., 2019), would have been initially C-poor, as C is incompatible (e.g., Shcheka et al., 2006). Thus, the narrow range of $\delta^{13}C$ in carbonates from Mount Hochwart (Fig. 3a) likely reflects that of the infiltrating COH fluid. Its low $\delta^{13}C$ may be achieved when carbonate-equilibrated COH fluid equilibrates with graphite (e.g., Cook-Kollars et al., 2014) or vice versa (e.g. Tumiati et al., 2022), particularly at high *T*. Conversely, the trend of relatively constant $\delta^{13}C$ but varying $\delta^{18}O$ for dolomite in Mount Hochwart peridotite (Fig. 3a) suggests initial buffering of the COH fluid $\delta^{18}O$ to mantle values when fluid-rock ratios were low, and its evolution to heavier $\delta^{18}O$ at increasing fluid-rock ratios. The fluid in equilibrium with the isotopically heaviest dolomite ($\delta^{18}O$ of +10.4‰) would have had a $\delta^{18}O$ of +5.2‰ to +5.4‰ (Text S1), which is a minimum estimate if it was still partially equilibrated with mantle oxygen. Such isotopically heavier O may be sourced from a variety of crustal rocks, such as carbonates, clays and sandstones (with decreasing average $\delta^{18}O$; Bindeman, 2008).

Late-stage calcite veinlets are not restricted to fine-grained Stage-3 or −4 peridotites, and are also observed in coarse-grained peridotites representing earlier stages (Consuma et al., 2020). A given whole-rock analysis may therefore contain several carbonate generations with distinct C—O isotopic compositions, meaning that isotopic distinctions between early vs. late carbonates will be muted. Nevertheless, some regularities are evident: Calcite veins, which are always texturally late, and calcite-brucite intergrowths after dolomite (Fig. 2b) are on average isotopically heavier than discrete dolomite (Fig. 3a). Modelling shows that Rayleigh-style dedolomitisation at 400 °C (representative of exhumation; see Fig. 1b), can reproduce the trend formed by matrix dolomite (Fig. 3a inset; see Text S1 for modelling details). Conversely, the very low $\delta^{13}C$-$\delta^{18}O$ of late magnesite veins and of dolomite associated with a serpentine vein (Fig. 3a) may reflect formation from a late graphite- and mantle-equilibrated fluid.

5.2. Strong provinciality of COH fluid composition

When carbonate $\delta^{13}C$-$\delta^{18}O$ values are cast with respect to geographic domain rather than carbonate type (Fig. 3b), it is evident that carbonate minerals from localities in the SW Ulten Zone domain have higher $\delta^{13}C$ and $\delta^{18}O$ (–11.2‰ to 0‰ and +12.7‰ to +20.7‰, respectively) than carbonate minerals from localities in the NE domain (–14.6‰ to –5.7‰ and +9.9‰ to +17.8‰, respectively). Because, at the modelled conditions, the observed range in carbonate $\delta^{13}C$-$\delta^{18}O$ is difficult to achieve via Rayleigh-style fractionation and devolatilisation (e.g. modelling in Fig. 3a inset), this marked provinciality points to involvement of an isotopically distinct COH fluid for peridotites from the SW domain, the carbonate inventory of which is dominated by late, isotopically heavy calcite (Fig. 3a). This interpretation is consistent with the observation that samples from the SW domain (e.g., Malga Preghena, Malga Binasia) tend to be more strongly retrogressed than those from the NE domain (e.g., Samerbergalm, Mount Hochwart), and with the distinctly more radiogenic $^{87}Sr/^{86}$ Sr for vein dolomite than matrix dolomite (Consuma et al., 2020). During tectonic uplift of the Ulten Zone tectonic mélange to midcrustal levels (Ranalli et al., 2005), the peridotites in the SW domain may have interacted with fluids locally derived from an adjacent ophiolitic suite containing isotopically heavy ophicarbonates (those from various localities in the Alps and Apennines have $\delta^{13}C$ of ~0‰ ± 4‰; Collins et al., 2015; Scambelluri et al., 2016). Ophicarbonate is exposed close to the SW domain and may represent portions of an ancient subducted slab of old oceanic lithosphere predating the Variscan continental collision (Martin et al., 1998, references therein). In contrast, the peridotites from the NE domain remained largely unaffected by this process, due to their greater distance to the ophiolitic suite.

The geographic distinctness described above adds to earlier discussions of a provinciality detected between ultramafic samples from Samerbergalm vs. those from Seefeldalm and Malga Masa Murada: The strongest fluid imprint, in the central domain, is expressed by high LILE contents, HREE loss due to garnet-breakdown, addition of enriched Nd-Hf and kinetically fractionated Li isotope compositions accompanying Li addition (Gudelius et al. 2019, 2022). This shows that significant differences exist at the scale of 10 s of km in a given tectonic mélange, which only came to light during more recent field campaigns (Förster et al., 2017; Gudelius et al., 2019), and highlights the necessity of comprehensive sampling in the field.

5.3. Carbon gain during near-peak-metamorphic interaction of crustal fluid with continental mantle wedge peridotite

Overall, the bulk C concentrations of Ulten Zone peridotites (130 to 2800 μg g^{-1}, median 610 μg g^{-1}) markedly exceed those of estimates for either convecting mantle (110±40 μg g^{-1}; Hirschmann, 2018) or average off-cratonic continental mantle (93±61 μg g^{-1}; Gibson and McKenzie, 2023). Combined with radiogenic Sr isotopic signatures of Ulten Zone carbonates and similar $^{87}Sr/^{86}Sr$ in coexisting amphibole (Consuma et al., 2020, 2021), this indicates that the lithospheric mantle wedge was enriched by a crustal COH fluid. The four crustal samples (2 migmatites, 2 gneisses with pelite protoliths; Hauzenberger et al., 1996) have C concentrations ranging from 500 to 2200 μg g^{-1} (Table S5), despite being high-grade metamorphic rocks that are typically devolatilised (e.g., Cook-Kollars et al., 2014). Rayleigh distillation modelling (Text S1) suggests that devolatilisation may have contributed to, but is insufficient to explain, their low measured bulk-rock $\delta^{13}C$ (−25.4‰ to −33.0‰). This points to the presence of graphite in the crustal source, which is, in fact observed in the metasedimentary rocks of the Ulten Zone (Martin et al., 2009).

The distinctness of carbonates from the NE and SW domain peridotites, discussed in the previous section, is confirmed in a plot of bulk-rock content vs. bulk $\delta^{13}C$ (Fig. 4a). The NE-domain peridotites show a distinct trend of strong C gain at variable $\delta^{13}C$. In contrast, SW-domain peridotites show a trend of weak C gain, but significant evolution in $\delta^{13}C$. They are in part overlapped by peridotites from the central domain, the latter of which are, however, restricted to a narrower range of values. Rayleigh fractionation modelling (see Text S1 for rationale and details) for temperatures representative of the early Ulten Zone evolutionary stages (800–600 °C; Fig. 1b) shows that the NE domain trend is captured when dolomite is added from a moderately C-rich fluid at high temperature (e.g., 700 °C), resulting in a strong carbon gain at small $\delta^{13}C$ variation. In contrast, the SW domain trend is captured when calcite is added at low temperature (e.g., 400 °C) from a fluid having lower CO_2/H_2O.

5.4. Carbon loss and increasing fraction of a ^{13}C-depleted phase during exhumation

A third trend in Fig. 4a, of strongly decreasing $\delta^{13}C$ at moderately decreasing C concentration, is plausibly associated with dedolomitisation manifested as calcite-brucite intergrowths replacing dolomite (Förster et al., 2017), therefore assignable to Stage 4. This trend can be modelled by Rayleigh-style calcite loss at low temperature (400 °C), representative of the serpentinisation stage. Reproducing the lowest $\delta^{13}C$ additionally requires that a ^{13}C-depleted component, such as graphite, be present in the rock (Fig. 4b; see Text S1 for rationale and details). Indeed, almost all bulk-rock $\delta^{13}C$ values are lower than those of associated bulk carbonate leachates (Fig. 5a). The difference is on average higher for peridotites from the SW domain (median $\delta^{13}C$ difference between carbonate and bulk-rock, $\Delta^{13}C_{carb\text{-}WR} = 3.0‰$) than for those from the NE domain (median $\Delta^{13}C_{carb\text{-}WR} = 2.2‰$). This is taken to indicate that, besides the carbonate minerals, one or more additional C-bearing species occur in the Ulten Zone peridotites, which lower/s the whole-rock $\delta^{13}C$ signature. The greater degree of serpentinisation-related alteration in SW-domain peridotites, possibly attended by more reducing conditions, may be favourable to graphite

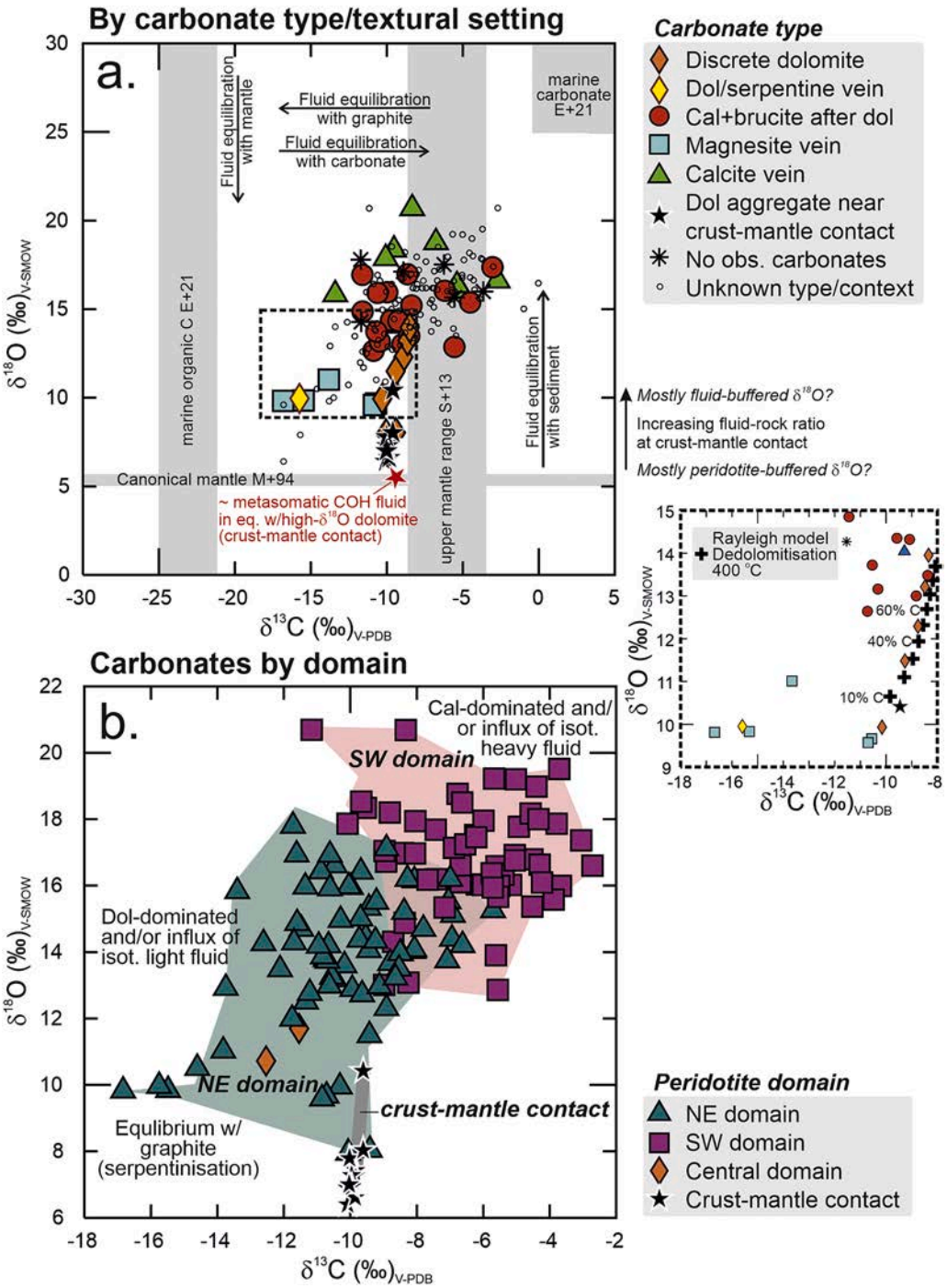

Fig. 3. Carbon-oxygen isotope relationships in carbonate minerals from the Ulten zone shown according to a. carbonate mineral and textural setting, and b. geographic domain (Fig 1a) (dol – dolomite, cal – calcite, obs – observed, isot – isotopically, eq - equilibrium). a. Equilibration of the COH fluid with mantle peridotite or sediment would cause a decrease and increase in $\delta^{18}O$, respectively; equilibration of the fluid with graphite or carbonate would cause $\delta^{13}C$ to decrease and increase, respectively. Rayleigh-style devolatiliation would cause the residual dolomite to evolve to lighter isotope compositions, as shown in inset (stippled box) and modelled for initial $\delta^{13}C$ of −8‰ and $\delta^{18}O$ of +14‰; numbers next to crosses denote the %C remaining as dolomite (see Text S1 and Table S7 for modelling details). The evolution of Mount Hochwart dolomite to higher $\delta^{18}O$ at near-constant $\delta^{13}C$ may reflect evolution of a sediment-equilibrated COH fluid from initial buffering to close to peridotite $\delta^{18}O$ values at low to increasingly higher fluid-rock ratios, whereas the $\delta^{13}C$ of the initially C-depleted peridotite would have been instantly overprinted. A metasomatic fluid in equilibrium with dolomite (red star) having $\delta^{18}O$ of +10.4‰ and $\delta^{13}C$ of −10.0‰ would have $\delta^{18}O$ of ~+5.3‰ and $\delta^{13}C$ of ~−5.0‰ at 660–700 °C estimated for this crust-mantle contact (Tumiati et al., 2007; Marocchi et al., 2009). Canonical mantle range for $\delta^{13}C$ from Shirey et al. (2013; $S + 13$) and for $\delta^{18}O$ from Mattey et al. (1994; $M + 94$), marine inorganic and carbonate carbon from Epstein et al. (2021; $E + 21$). b. Distinct distributions for carbonates from the NE vs. the SW Ulten Zone domain, whereby the carbonate inventory of the former is suggested to be dominated by dolomite whereas that of the latter is dominated by calcite. Given the limited range of isotopic fractionation by Rayleigh-type devolatilisation (see inset), the influx of isotopically distinct fluids in the two domains seems likely.

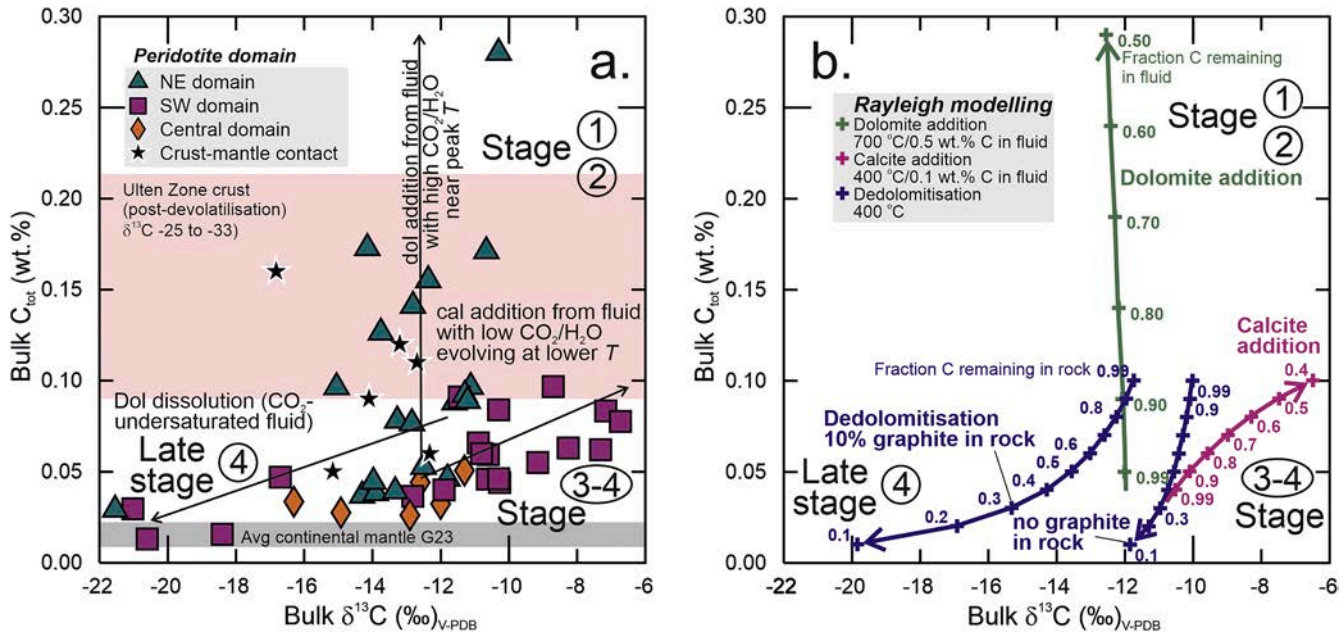

Fig. 4. Bulk-rock carbon concentrations and isotopic compositions shown according to geographic domain (dol – dolomite, cal – calcite). a. Bulk-rock $\delta^{13}C$ vs. carbon concentration. Three trends are identified and tentatively correlated to the metamorphic evolution (stages 1–4) of Ulten Zone peridotites (see Fig. 1b). Shown for comparison is the carbon concentration range for four Ulten Zone crustal rocks (this work, $\delta^{13}C$ range is also indicated) and average off-cratonic continental value from Gibson and McKenzie (2023; G23). b. Rayleigh distillation modelling designed to reproduce the suggested trends (see Text S1 and Table S7 for modelling details): Trend 1 + 2 models Rayleigh-style dolomite addition at 700 °C with a starting $\delta^{13}C$ of −12‰ and C concentration of 0.04 wt. %, and capacity of the fluid to precipitate 0.5 wt. % C as dolomite (higher T will result in even smaller $\delta^{13}C$ variation whereas higher C in the fluid will result in a stronger C gain per modelled C fraction interval); Trend 3 models Rayleigh-style calcite addition at 400 °C, also with a starting $\delta^{13}C$ of −12‰ and C concentration of 0.04 wt. %, and capacity of the fluid to precipitate 0.1 wt. % C as calcite; Trend 4 models Rayleigh-style dedolomitisation at 400 °C with a starting $\delta^{13}C$ of −10‰ and C concentration of 0.1 wt. % (corresponding to an initially mildly enriched rock), whereby the residue is modelled as pure inorganic C (no graphite in rock), and alternatively as a mixture of 90% inorganic C and 10% graphite (assuming $\delta^{13}C$ of −27‰) in the residual rock, as one explanation to explain the $\delta^{13}C$ difference between measured whole rocks and their corresponding carbonates shown in Fig. 5a.

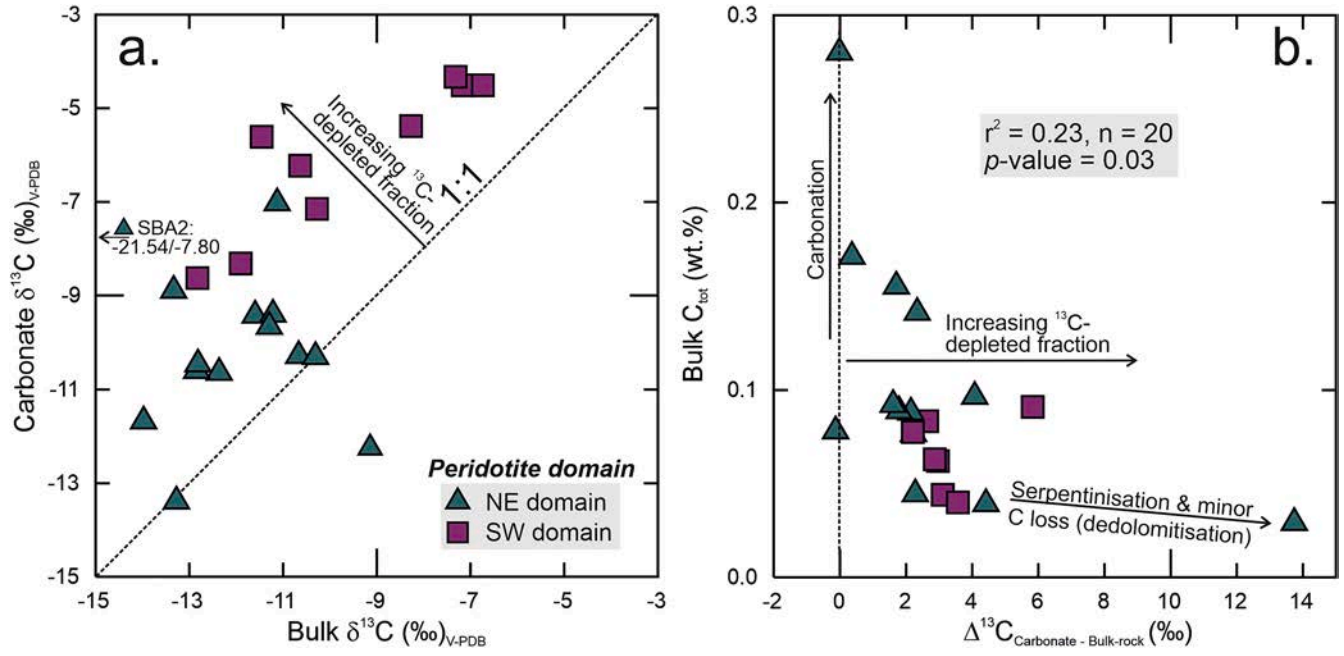

Fig. 5. a. Bulk-rock vs. carbonate $\delta^{13}C$. The mostly lower bulk-rock than carbonate $\delta^{13}C$ suggests the presence of a ^{13}C-depleted component, such as graphite or methane. A single outlying value is indicated with small symbol and arrow. b. Difference Δ between $\delta^{13}C$ measured in carbonate and that in corresponding bulk rocks, as a measure of graphite fraction in the bulk rock, vs. bulk-rock carbon concentration (wt. %). Amphibolitisation is acccompanied by a strong increase in carbon concentration, probably reflecting dolomite addition (dominantly NE domain; see Fig. 4), whereas serpentinitsation leads to a decrease in bulk-rock $\delta^{13}C$, accompanied by a higher fraction of a ^{13}C-depleted component, such as graphite or methane.

stability. Overall, the co-existence of both reduced and oxidised forms of C would be consistent with the fO_2 estimates of Gudelius et al. (2019) which lie near the graphite-CO_2 equilibrium (Fig. 1d), bearing in mind that in multi-component systems these univariant reaction curves will open up into divariant fields (e.g., Tumiati and Malaspina, 2019). However, graphite has yet to be directly identified in the assemblage. The low-$\delta^{13}C$ component might be present in the form of extremely fine-grained graphite not readily observed petrographically. If so, the average fraction of reduced C in Ulten Zone peridotites may be estimated at ~10%, assuming that graphite has a $\delta^{13}C$ of –27‰, similar to that of the average total reduced C in ophiolite-associated peridotites and serpentinites (Schwarzenbach et al., 2016). We note that, in the

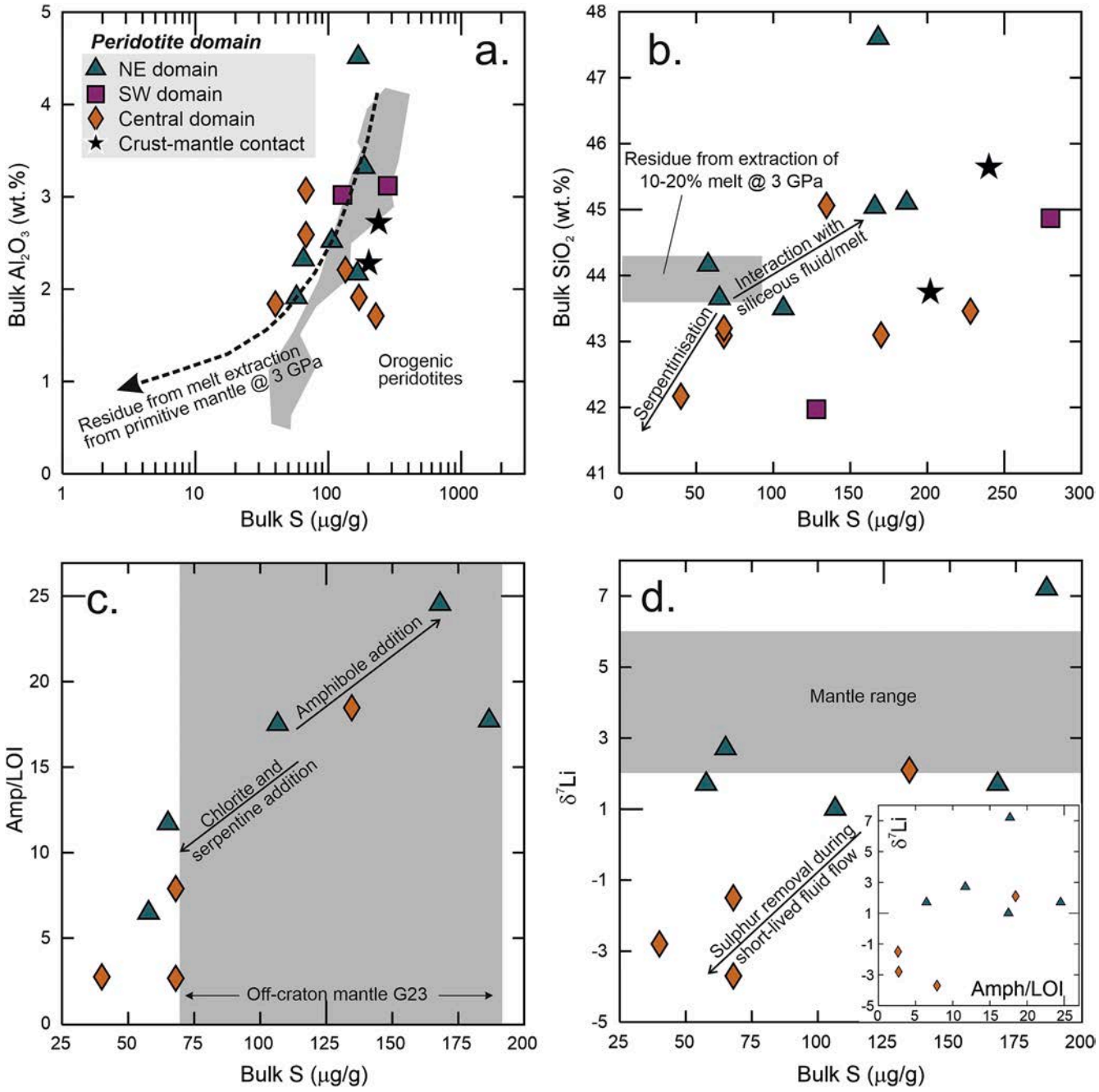

Fig. 6. Relationships of bulk-rock sulfur abundances (µg g^{-1}) in Ulten Zone peridotites (from Consuma et al., 2021) with various compositional and mineralogical parameters (from Gudelius et al., 2019; this study). a. Bulk-rock sulfur (note log scale) vs. Al_2O_3 concentration. Shown for comparison are the quantitatively modelled trend for melt extraction from a primitive mantle source at 3 GPa and the field for orogenic peridotites world-wide from Aulbach et al. (2016). Bulk-rock sulfur vs. b. SiO_2 concentration, possibly indicating addition during interaction with high-*P* siliceous fluid, and c. the ratio of amphibole modal abundance over Loss-On-Ignition (LOI) values, as a measure of the abundance of amphibole (Amph) vs. chlorite + serpentine. In b., grey field encompasses range of concentrations in a residue of 10–20% melting commencing at 3 GPa (S from Aulbach et al., 2016; SiO_2 from Herzberg, 2004), consistent with melt fraction and melting pressure estimates for Ulten Zone peridotites of Ionov et al. (2017) and Gudelius et al. (2019). In c., range of sulfur concentrations in off-cratonic lithospheric mantle from Gibson and McKenzie (2023; G23). d. Bulk-rock sulfur concentration vs. δ^7Li (in ‰), interpreted to reflect the transient ingress of crustal fluid, with addition of fluid-mobile elements including Li, and removal of the fluid source before isotopic equilibration could take place, leading to enrichment in ^{6}Li over ^{7}Li. Inset shows δ^7Li vs amph/LOI, confirming the exhumation-related nature of this event, with formation of chlorite and serpentine at the expense of amphibole. Mantle δ^7Li range from Ionov and Seitz (2008).

rocks studied by Schwarzenbach et al. (2016), high reduced C fractions (average ~0.5) are chemically derived, but not described as part of the observed assemblage. Circumstantial support for the presence of a reduced C component may come from the observation that C fractions released at 550 °C (possibly dominated by graphite) vs. those released at 1000 °C (possibly dominated by carbonate minerals) show some correlation with the difference between $\delta^{13}C$ values measured in carbonate vs. those in their corresponding bulk rocks (Fig. S6). Combined consideration of $Fe^{3+}/\Sigma Fe$ and C-S elemental and isotope systematics discussed below suggest some graphite may have formed by methane oxidation or carbonate reduction. An alternative repository of isotopically light C could be methane now trapped as fluid inclusions in minerals or a grain boundary component, generated from inorganic C at low temperature (<340 °C), a process suggested to be ubiquitous in olivine-bearing lithologies (Klein et al., 2019). Serpentinisation produces magnetite and hydrogen, and magnetite is thought to catalyse the reaction of hydrogen with dissolved CO_2 to produce methane (Cannat et al., 2010). This may explain the presence of magnetite associated with serpentine described in Consuma et al. (2021) and in this study, and provide a pathway for methane production in the samples. As is true for graphite, methane has yet to be identified in Ulten Zone peridotites.

Taking $\Delta^{13}C_{carb\text{-}WR}$ as a measure of the fraction of ^{13}C-depleted phases present in the rock, a weak but statistically significant negative correlation with bulk C concentration ($r^2 = 0.23$ for $n = 20$, p value = 0.03; Fig. 5b) seemingly confirms that increasing precipitation of reduced, isotopically light phases is accompanied by a net loss of isotopically heavy CO_2 to a fluid via devolatilisation (dedolomitisation).

5.5. Contrasting behaviour of sulfur during near-peak-metamorphic vs. exhumation stages

Consuma et al. (2021) investigated the $\delta^{34}S$ of sulphides in Ulten Zone peridotites and noted the intimate association of sulphides with carbonates, suggesting coupled introduction of C and S from crustal fluid carrying slightly heavy S and radiogenic Sr. Closer investigation of S abundance relationships with other compositional and mineralogical parameters allows to obtain ulterior insights into sulfur behaviour during the 4-stage metamorphic evolution of the Ulten Zone peridotites. Ionov et al. (2017) suggest that the pre-Variscan protolith to the Ulten Zone peridotites formed by polybaric melting initiating at 2–4 GPa and leading to a loss of 10–20% of melt, which is a minimum estimate if any subsequent refertilisation took place (Gudelius et al., 2019). The progressive removal of melt is accompanied by depletion of S, dictated by the sulphide solubility in the melt, and has been modelled for various pressures by Aulbach et al. (2016). Fig. 6a shows that more than half of the samples are as depleted as, or more depleted than, predicted for melt extraction, whereas the remaining samples are more enriched.

Although S concentrations in Ulten Zone peridotites remain below primitive mantle with ~250 μg g^{-1} S (McDonough and Sun, 1995), there is some evidence that S was metasomatically (re-)introduced after lithospheric stabilisation. Firstly, sulphide $\delta^{34}S$ indicates that some crustal sulphate-S was added and reduced to form sulphide (Consuma et al., 2021). There is a, albeit weak, positive correlation of bulk-rock S with SiO_2 concentrations (Fig. 6b). This suggests addition from a siliceous fluid during the high-P stage, when silica solubility in the fluid is higher than at lower P (e.g., Hermann et al., 2006) or during interaction with sediment-derived melt, as suggested for Mount Hochwart (Marocchi et al., 2009). Taking the ratio of amphibole mode over Loss-On-Ignition (amph/LOI) as a measure of the abundance of amphibole vs. chlorite and serpentine suggests that chloritisation and serpentinisation entailed S removal from the bulk rocks (Fig. 6c). This is consistent with the appearance of metal-rich sulphides during the exhumation and serpentinisation stages (Fig. 1c), which affected a greater proportion of peridotites from the central than from the NE domain.

At the fO_2 recorded by Ulten Zone peridotites, all S would be contained in sulphides (Fig. 1d), suggesting that S was removed as H_2S, which is possible when sufficient amounts of fluid are available (Jégo and Dasgupta, 2013). The positive correlation between amph/LOI and δ^7Li (Fig. 6d) documents that the fluid flow event leading to serpentinisation was transient. It led to addition of fluid-mobile elements, including Li, the isotopic composition of which was kinetically fractionated (with the light isotope travelling faster/further), with removal of the fluid before isotopic equilibration (with the heavy isotope catching up) could occur (Gudelius et al., 2019).

5.6. Iron-sulfur-carbon redox interactions in the mantle wedge

Iron, C and S are the most abundant multivalent elements involved in redox interactions in the mantle (e.g., Ballhaus, 1993; O'Neill et al., 1993). The high estimated Fe_2O_3 contents of Ulten Zone peridotites (average 1.7 wt. % ± 0.6 1σ) contrast with estimates for the Primitive Mantle (0.33 wt. %; Sossi et al., 2020). Moreover, Fe^{3+} has low solubility in aqueous fluids (Wykes et al., 2008), and bulk-rock total FeO contents vary little (7.9 ± 0.6 wt. %). Combined, this suggests that the fraction of Fe^{3+} was increased during redox interactions involving reduction of oxidised components, most likely carbon and sulfur. Although redox interactions involving several multi-valent elements are doubtlessly complex and may vary in response to small changes in P, T, X and fO_2, we suggest in the following a possible sequence of events and redox processes that takes into account all available data.

Again taking Amph/LOI as a measure for the presence of amphibole vs. chlorite and serpentine, it is evident that these latter minerals are associated with the highest $Fe^{3+}/\Sigma Fe$ (Fig. 7a). As discussed above, S addition occurred during the early near-peak-metamorphic stage, characterised by addition of siliceous fluid and amphibole (Fig. 6b,c). Combined with the presence of moderately heavy $\delta^{34}S$ in Ulten Zone sulphides (up to +3.43‰) and radiogenic Sr in spatially associated carbonates (Consuma et al., 2021), this points to a crustal COH fluid and an origin of a fraction of the sulphides by sulphate reduction, accompanied by oxidation of iron in peridotite minerals. Given that amphibole formed after clinopyroxene, a possible redox reaction could be (e.g., Evans and Tomkins, 2022):

$$SO_4^{2-}(\text{fluid}) + 8\,FeO(\text{pyroxene}) = S^{2-}(\text{sulphide}) + 4Fe_2O_3(\text{amphibole}) \quad (1)$$

Redox-neutral sulphidation and carbonation likely also played a role, exemplified by a sample from the crust-mantle contact at Mount Hochwart with simultaneously high sulfur and carbon concentrations, yet low $Fe^{3+}/\Sigma Fe$. Given that sulphide in Ulten Zone peridotites is dominantly pentlandite (Consuma et al., 2021), sulphidation may, in a general reaction, proceed via (Bataleva et al., 2016):

$$S^{2-}\ (\text{fluid}) + \text{Fe,Ni (olivine)} = S^{2-}\text{,Fe,Ni (pentlandite)} \quad (2)$$

Redox-neutral carbonation may proceed via (Wyllie et al., 1983):

$$2\ CO_2\ (\text{fluid}) + 2\ MgSiO_4\ (\text{olivine}) + CaMgSi_2O_6\ (\text{diopside}) = CaMg(CO_3)_2\ (\text{dolomite}) + 4\ MgSiO_3\ (\text{enstatite}) \quad (3)$$

The highest $Fe^{3+}/\Sigma Fe$ are associated with low S concentrations (Fig. 7b), which reflects desulphidation, as also indicated by the appearance of metal-rich sulphides during the exhumation-related metamorphic stages (Fig. 1c) (Consuma et al., 2021). This, in turn, suggests that redox interactions involving iron oxidation during chloritisitation and serpentinisation instead involved carbonate reduction, such as, in a general reaction:

$$MgCO_3\ (\text{magnesite}) \text{ or } CaCO_3\ (\text{calcite}) + FeO\ (\text{olivine}) = C\ (\text{graphite}) + Fe_2O_3\ (\text{chlorite, serpentine}) \quad (4)$$

bearing in mind the late appearance of magnesite and calcite along with chlorite and serperpentine, respectively, in the assemblage (Fig. 1c) (Consuma et al., 2021).

This would be consistent with indirect evidence for the presence of a

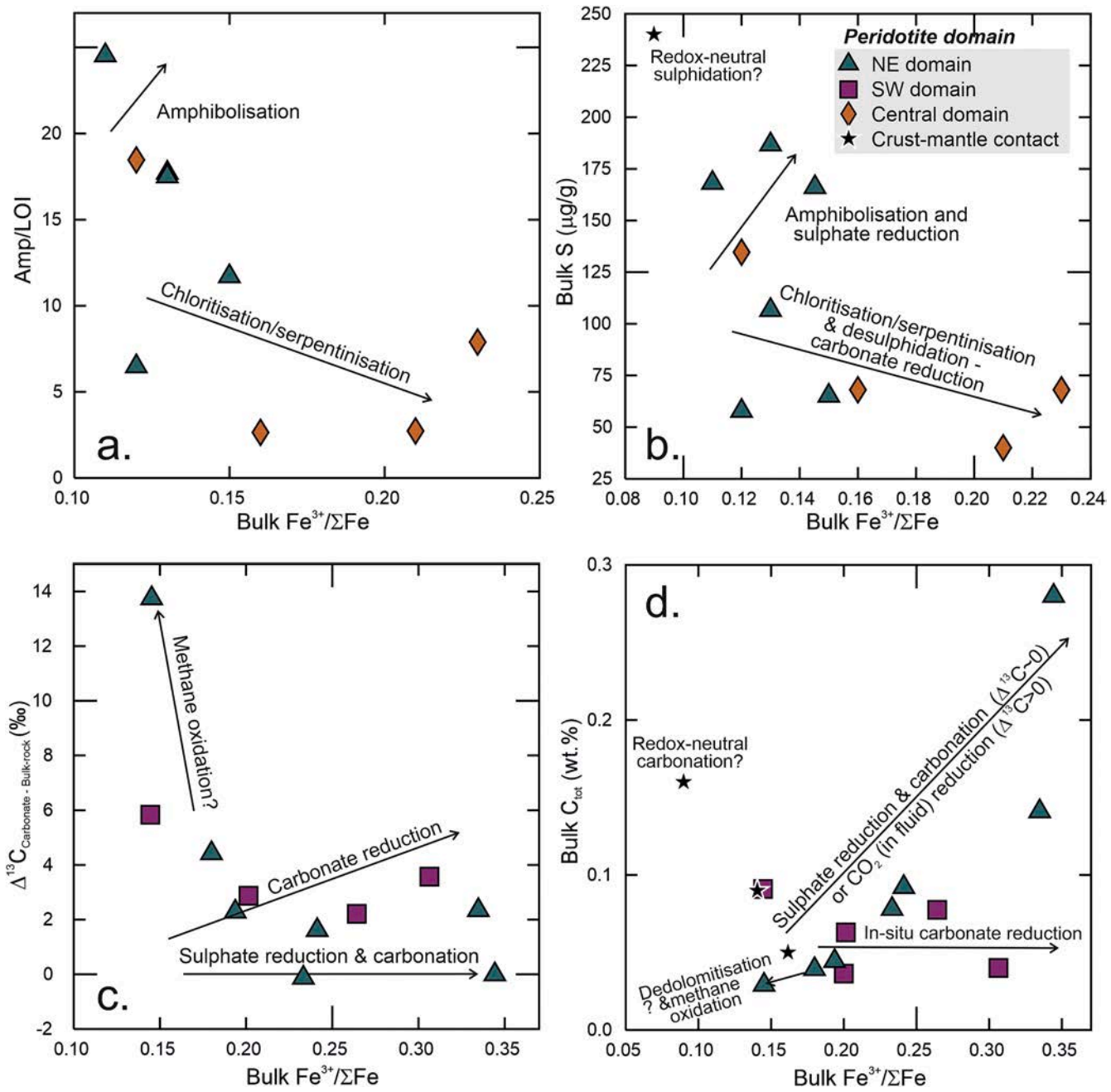

Fig. 7. Bulk-rock $Fe^{3+}/\Sigma Fe$ vs. a. Amph/LOI as a measure of amphibole vs. chlorite+serpentine, b. sulfur concentration (µg g^{-1}), c. $\Delta^{13}C_{carb\text{-}WR}$ and d. bulk-rock carbon concentration (wt.%). In a., both amphibolitisation during stage one and chloritisation/serpentinisation during stages 2 and 3 would lead to an increase in $Fe^{3+}/\Sigma Fe$ if accompanied by the reduction of oxidised sulfur or carbon, given that Fe^{3+} is considered not fluid-soluble (Wykes et al., 2008). Compared to serpentine, chlorite dominates the Fe^{3+} budget owing to its potentially high total Fe content (Masci et al., 2019). In b., amphibolitisation may have been accompanied by sulphate reduction (indicated by supra-mantle sulphide $\delta^{34}S$; Consuma et al., 2021); the low sulfur concentration at high $Fe^{3+}/\Sigma Fe$, coinciding with low Amph/LOI, suggests desulphidation (low fS_2) during exhumation-related metamorphic stages, making carbonate rather than sulphate reduction the most likely process to increase sample $Fe^{3+}/\Sigma Fe$ (at relatively constant FeO^{total}, see text). This would be consistent with the presence of a graphite fraction inferred from the difference (Δ) between $\delta^{13}C$ measured in carbonate and that in corresponding bulk rocks shown in panel c. In contrast, increasing $Fe^{3+}/\Sigma Fe$ at low $\Delta^{13}C_{carb\text{-}WR}$ would indicate sulphate reduction and redox-neutral carbonation. Simultaneously high $\Delta^{13}C_{carb\text{-}WR}$ and low $Fe^{3+}/\Sigma Fe$ may point to conditions reducing enough to permit graphite formation from fluid-advected methane, most likely during serpentinisation, which can also explain the low carbon content at low $Fe^{3+}/\Sigma Fe$ in d. because serpentinisation is associated with decarbonation (see Fig. 4a). In d., carbonation accompanied by sulphate reduction (explaining the spatial association of sulphides and carbonates noted by Consuma et al., 2021) or reduction of fluid-advected CO_2 can explain simultaneously high carbon contents and $Fe^{3+}/\Sigma Fe$. In contrast, increasing $Fe^{3+}/\Sigma Fe$ without increasing carbon content may point to in-situ carbonate reduction catalysed by fluid, whereas low $Fe^{3+}/\Sigma Fe$ and carbon content may reflect dedolomitisation.

^{13}C-depleted phase, such as graphite, which is more pronounced for the SW-domain than for the NE-domain peridotites (Fig. 5). Thus, sulphate reduction explains high $Fe^{3+}/\Sigma Fe$ at low fractions of a ^{13}C-depleted phase (graphite or methane) gauged by $\Delta^{13}C_{carb\text{-}WR}$. In contrast, carbonate reduction, with preferential export of isotopically heavy C, would have led to a concomitant increase in $Fe^{3+}/\Sigma Fe$ and in fractions of a ^{13}C-depleted phase, although a trend is not recognisable (Fig. 7c). For the case of relatively constant C concentration at variable $Fe^{3+}/\Sigma Fe$, as

seen in SW-domain peridotites (Fig. 7d), fluid-catalysed *in-situ* reduction of carbonate as per Eq. (4) may be indicated. In contrast, low $Fe^{3+}/\Sigma Fe$ at high $\Delta^{13}C_{carb\text{-}WR}$ (Fig. 7c) and low bulk carbon content (Fig. 7d) suggests the presence of a graphite fraction that may have formed due to reduction of iron by methane oxidation. This scenario would be permitted by reducing conditions that are frequently linked to serpentinisation (e.g., Evans et al., 2023). The findings are summarised – in a simplified manner – in Fig. 8, bearing in mind the scatter observed in data, which is expected given that each sample is to varying extents the product of the superposition of multiple metamorphic events.

5.7. *Implications for volatile element storage in continental collisional settings*

Continental subduction zones are probable sites for the reintroduction of volatile elements into originally depleted lithospheric mantle, via recycling from subducted slabs that can be probed by sampling exhumed orogenic peridotite. If data from the Ulten Zone tectonic mélange are representative, then processes occurring near peak-metamorphic conditions in the mantle wedge (stages 1 and 2 in Fig. 8) lead to a replenishment of S stored in sulphide, and to significant enrichment of C stored in carbonate and of water stored in amphibole. If the mantle wedge stabilises subsequent to collision, it would represent a sizable volatile element-rich reservoir. Indeed, huge swaths of lithospheric mantle now underlying continental interiors stabilised in accretionary orogens and continental collision zones, such as the massive Central Asian and the Alpine-Himalayan orogenic belts, and countless older examples. Stage-1, and stage-2 peridotites may also be useful proxies of mantle wedge peridotites that are dragged down to sub-arc depths, where they contribute to arc magmas, or recycled deeper into the convecting mantle, where they cause compositional and mineralogical heterogeneity. Such volatile element-enriched peridotite may contribute to later continental magmatism and ore formation. For example, Variscan subduction-modified mantle has been invoked to explain the occurrence of calc-alkaline to shoshonitic Triassic magmas in the Southern Alps (Casetta et al., 2021). This is not an isolated observation, as crustal C addition to the mantle wedge beneath the Betic Cordillera (Spain), as a precursor to the genesis of calc-alkaline to potassic magmas (lamproites), is similarly suggested (Bianchini et al., 2015; Bianchini and Natali, 2017). Subduction-modified continental lithospheric mantle has recently been implicated in the formation of giant gold deposits in eastern China based on isotopically heavy S and enriched Sr-Nd isotope compositions in lamprophyres (Wang et al., 2024) – characteristics shared with the Ulten Zone peridotites.

6. Summary and conclusions

We investigated the major-element composition, Fe speciation, and C concentration and isotope composition of ultramafic whole rocks from the Ulten Zone, as well as the C and O isotope composition of the carbonate minerals they contain. These rocks experienced a four-stage evolution encompassing (1) a precollisional stage with residence in the hot mantle wedge, (2) a high-*P* stage due to down-dragging with the subducting slab accompanied by cooling and amphibolitisation, (3) early fast exhumation and chloritisation and (4) late slow exhumation and serpentinisation. Combined with literature data, our main findings are as follows:

- Bulk-rock C and Fe_2O_3 contents range from 130 to 28,000 μg g^{-1} and from 0.8 to 3.1 wt. %, respectively, all exceeding estimates for the convecting mantle; reported bulk-rock S contents range from 30 to 330 μg g^{-1}, mostly remaining below estimates for the convecting mantle, but partly higher than those expected for residual lithospheric mantle.
- Bulk-rock C contents are on average higher in rocks from the NE domain (median 880 μg g^{-1}) than for the SW domain (median 570 μg g^{-1}). Carbonate stable isotope compositions also show distinct isotopic compositions, as rocks from the NE Ulten Zone domain have lower average $\delta^{13}C_{V\text{-}PDB}$ and $\delta^{18}O_{V\text{-}SMOW}$ (–16.8‰ to –5.7‰ and +8.0‰ to +17.8‰, respectively) than those in the SW domain (–11.2‰ to 0‰ and +12.9‰ to +20.7‰, respectively), likely reflecting interaction with isotopically distinct crustally-derived fluids.
- Texturally late-stage calcite veins are isotopically heavier than dolomite and slightly heavier than those affected by dedolomitisation (leading to characteristic pseudomorphs of calcite + brucite after dolomite).
- Lower $\delta^{13}C$ values for whole rocks than for carbonate (by 2.3‰ on average) provide indirect evidence for the presence of ^{13}C-depleted reduced C. This is tentatively suggested to be graphite or methane, neither of which has been directly observed, but helps explain some elements of the dataset for bulk-rock $Fe^{3+}/\Sigma Fe$, $\delta^{13}C$ and C-S concentrations.
- Bearing in mind the scatter arising from multiple metamorphic overprints, the data in combination suggest that $Fe^{3+}/\Sigma Fe$ and sulphide abundances increased during amphibolitisation due to sulphate reduction, as well as by redox-neutral sulphidation and carbonation. In contrast, chloritisation was accompanied by an increase in $Fe^{3+}/\Sigma Fe$ mediated by carbonate reduction, leading to an increase in the inferred graphite fraction. Highly reducing conditions during serpentinisation led to a decrease in $Fe^{3+}/\Sigma Fe$, possibly via

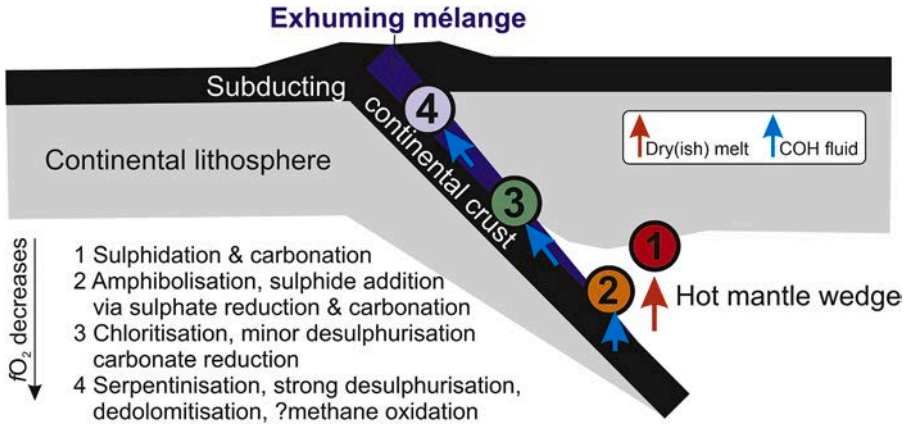

Fig. 8. Cartoon summarising the loci of processes during the four main metamorphic stages (see Fig. 1b,c) leading to volatile element addition and removal in the Ulten Zone continental mantle wedge, as inferred from $Fe^{3+}/\Sigma Fe$ as well as sulfur-carbon elemental and isotopic relationships shown in Fig. 7.

methane oxidation, and an increase in the inferred graphite fraction that did not compensate the C loss caused by dedolomitisation.
- If carbonation and amphibolitisation near peak-metamorphic conditions are characteristic for continental mantle wedges, their subsequent stabilisation may promote long-term storage of C and H_2O in this tectonic setting, which characterises vast areas of Earth's continents and therefore may constitute a particularly volatile element-rich lithospheric reservoir.
- The mineralogical, geochemical and isotopic variability is observed not only at the outcrop scale, but also regionally at the scale of 10 s of kilometres in a single tectonic mélange. This indicates that comprehensive sampling of multiple ultramafic lenses is necessary to constrain the volatile element fluxes and storage associated with the multiple metamorphic stages experienced by exhumed orogenic peridotites.

CRediT authorship contribution statement

Bibiana Förster: Writing – review & editing, Writing – original draft, Visualization, Validation, Methodology, Investigation, Formal analysis, Data curation. **Sonja Aulbach:** Writing – original draft, Visualization, Supervision, Methodology, Formal analysis, Data curation, Conceptualization. **Gray E. Bebout:** Writing – review & editing, Validation, Supervision, Resources, Methodology, Investigation, Funding acquisition, Formal analysis, Conceptualization. **Gianluca Bianchini:** Writing – review & editing, Validation, Resources, Methodology, Investigation, Formal analysis. **Claudio Natali:** Writing – review & editing, Validation, Methodology, Investigation, Formal analysis. **Roberto Braga:** Writing – review & editing, Supervision, Resources, Project administration, Investigation, Funding acquisition, Conceptualization.

Declaration of competing interest

The authors declare that they have no known competing financial interests or personal relationships that could have appeared to influence the work reported in this paper.

The author is an Editorial Board Member/Editor-in-Chief/Associate Editor/Guest Editor for *[Chemical Geology]* and was not involved in the editorial review or the decision to publish this article.

Acknowledgments

We thank Dr. Bruce Idleman at Lehigh University for assistance with the SEM work and with the experimentation with methods for reaction of various carbonate phases to quantitatively release CO_2 for O—C isotope measurements. Thanks also are due to Enrico Cannaò, who contributed with valuable discussions and assisted, at all stages, with the stable isotope analyses at Lehigh University. The manuscript benefited from seamless handling by the editor, Fangzhen Teng, and was significantly improved by incisive comments from two anonymous reviewers. The stable isotope work conducted at Lehigh University was largely supported by National Science Foundation EAR-1119264 (to GEB). SA gratefully acknowledges funding by the German Research Foundation (project number 467591567).

Supplementary materials

Supplementary material associated with this article can be found, in the online version, at doi:10.1016/j.epsl.2024.119074.

Data availability

All new data will be provided as Supplementary Information (multiple sheets in one Excel file).

References

Aulbach, S., 2019. Cratonic lithosphere discontinuities: dynamics of small-volume melting, meta-cratonisation and a possible role for brines. In: Yuan, H., Romanowicz, B. (Eds.), Lithospheric Discontinuities. American Geophysical Union. John Wiley & Sons, pp. 177–204.
Aulbach, S., Mungall, J.E., Pearson, D.G., 2016. Distribution and Processing of Highly Siderophile Elements in Cratonic Mantle Lithosphere. High. Sideroph. Strong. Chalcoph. Element. High-Temp. Geochem. Cosmochem. 81, 239–304.
Ballhaus, C., 1993. Redox states of lithospheric and asthenospheric upper-mantle. Contribut. Mineral. Petrol. 114, 331–348.
Bataleva, Y.V., Palyanov, Y.N., Borzdov, Y.M., Sobolev, N.V., 2016. Sulfidation of silicate mantle by reduced S-bearing metasomatic fluids and melts. Geology 44, 271–274.
Bekaert, D.V., Turner, S.J., Broadley, M.W., Barnes, J.D., Halldórsson, S.A., Labidi, J., Wade, J., Walowski, K.J., Barry, P.H., 2021. Subduction-driven volatile recycling: a global mass balance. Annu. Rev. Earth Planet Sci. 49, 37–70.
Bianchini, G., Braga, R., Langone, A., Natali, C., Tiepolo, M., 2015. Metasedimentary and igneous xenoliths from Tallante (Betic Cordillera, Spain): inferences on crust–mantle interactions and clues for post-collisional volcanism magma sources. Lithos 220-223, 191–199.
Bianchini, G., Natali, C., 2017. Carbon elemental and isotopic composition in mantle xenoliths from Spain: insights on sources and petrogenetic processes. Lithos 272-273, 84–91.
Bindeman, I., 2008. Oxygen isotopes in mantle and crustal magmas as revealed by single crystal analysis. Rev. Mineral. Geochem. 69, 445–478.
Cannat, M., Fontaine, F., Escartin, J., 2010. Serpentinization and associated hydrogen and methane fluxes at slow spreading ridges. Geophys. Monogr. Ser. 188, 241–264.
Casetta, F., Ickert, R.B., Mark, D.F., Giacomoni, P.P., Bonadiman, C., Ntaflos, T., Zanetti, A., Coltorti, M., 2021. The Variscan subduction inheritance in the Southern Alps Sub-Continental Lithospheric Mantle: clues from the Middle Triassic shoshonitic magmatism of the Dolomites (NE Italy). Lithos 380-381, 105856.
Collins, N.C., Bebout, G.E., Angiboust, S., Agard, P., Scambelluri, M., Crispini, L., John, T., 2015. Subduction zone metamorphic pathway for deep carbon cycling: II. Evidence from HP/UHP metabasaltic rocks and ophicarbonates. Chem. Geol. 412, 132–150.
Consuma, G., Aulbach, S., Braga, R., Martin, L.A.J., Tropper, P., Gerdes, A., Fiorentini, M. L., 2021. Multi-stage sulfur and carbon mobility in fossil continental subduction zones: new insights from carbonate-bearing orogenic peridotites. Geochim. Cosmochim. Acta 306, 143–170.
Consuma, G., Braga, R., Giovanardi, T., Bersani, D., Konzett, J., Lugli, F., Mazzucchelli, M., Tropper, P., 2020. In situ Sr isotope analysis of mantle carbonates: constraints on the evolution and sources of metasomatic carbon-bearing fluids in a paleo-collisional setting. Lithos 354-455, 105334.
Cook-Kollars, J., Bebout, G.E., Collins, N.C., Angiboust, S., Agard, P., 2014. Subduction zone metamorphic pathway for deep carbon cycling: I. Evidence from HP/UHP metasedimentary rocks, Italian Alps. Chem. Geol. 386, 31–48.
Cottrell, E., Birner, S.K., Brounce, M., Davis, F.A., Waters, L.E., Kelley, K.A., 2022. Oxygen fugacity across tectonic settings. Magma Redox Geochem. 33–61.
Debret, B., Andreani, M., Muñoz, M., Bolfan-Casanova, N., Carlut, J., Nicollet, C., Schwartz, S., Trcera, N., 2014. Evolution of Fe redox state in serpentine during subduction. Earth Planet. Sci. Lett. 400, 206–218.
Debret, B., Reekie, C.D.J., Mattielli, N., Beunon, H., Ménez, B., Savov, I.P., Williams, H. M., 2020. Redox transfer at subduction zones: insights from Fe isotopes in the Mariana forearc. Geochem. Perspect. Lett. 12, 46–51.
Epstein, G.S., Bebout, G.E., Angiboust, S., 2021. Fluid and mass transfer along transient subduction interfaces in a deep paleo-accretionary wedge (Western Alps). Chem. Geol. 559, 119920.
Evans, K.A., Frost, B.R., Reddy, S.M., Brown, T.C., 2023. Causes, effects, and implications of the relationships amongst fluids, serpentinisation, and alloys. Lithos 446-447, 107132.
Evans, K.A., Tomkins, A.G., 2022. Redox variables and mechanisms in subduction magmatism and volcanism. Magma Redox Geochem. 63–91.
Foley, S.F., Fischer, T.P., 2017. An essential role for continental rifts and lithosphere in the deep carbon cycle. Nat. Geosci. 10, 897–902.
Förster, B., Braga, R., Aulbach, S., Lo Po, D., Bargossi, G.M., Mair, V., 2017. A petrographic study of carbonate phases in the Ulten Zone ultramafic rocks: insights into carbonation in the mantle wedge and exhumation-related decarbonation. Ofioliti 42, 105–127.
Gibson, S.A., McKenzie, D., 2023. On the role of Earth's lithospheric mantle in global volatile cycles. Earth Planet. Sci. Lett. 602, 117946.
Gibson, S.A., Rooks, E.E., Day, J.A., Petrone, C.M., Leat, P.T., 2020. The role of sub-continental mantle as both "sink" and "source" in deep Earth volatile cycles. Geochim. Cosmochim. Acta 275, 140–162.
Godard, G., Martin, S., Prosser, G., Kienast, J.R., Morten, L., 1996. Variscan migmatites, eclogites and garnet-peridotites of the Ulten zone, Eastern Austroalpine system. Tectonophysics 259, 313–341.
Gudelius, D., Aulbach, S., Braga, R., Hofer, H.E., Woodland, A.B., Gerdes, A., 2019. Element transfer and redox conditions in continental subduction zones: new insights from peridotites of the Ulten Zone, North Italy. J. Petrol. 60, 231–268.
Gudelius, D., Aulbach, S., Seitz, H.-M., Braga, R., 2022. Crustal fluids cause strong Lu-Hf fractionation and Hf-Nd-Li isotopic provinciality in the mantle of continental subduction zones. Geology 50, 163–168.
Hauzenberger, C.A., Höller, W., Hoinkes, G., 1996. Transition from eclogite to amphibolite-facies metamorphism in the Austroalpine Ulten Zone. Mineral. Petrol. 58, 111–130.

Hermann, J., Spandler, C., Hack, A., Korsakov, A.V., 2006. Aqueous fluids and hydrous melts in high-pressure and ultra-high pressure rocks: implications for element transfer in subduction zones. Lithos 92, 399–417.
Herzberg, C., 2004. Geodynamic information in peridotite petrology. J. Petrol. 45, 2507–2530.
Hirschmann, M.M., 2018. Comparative deep Earth volatile cycles: the case for C recycling from exosphere/mantle fractionation of major (H2O, C, N) volatiles and from H2O/Ce, CO2/Ba, and CO2/Nb exosphere ratios. Earth Planet. Sci. Lett. 502, 262–273.
Ionov, D.A., Bigot, F., Braga, R., 2017. The provenance of the lithospheric mantle in continental collision zones: petrology and geochemistry of peridotites in the Ulten-Nonsberg Zone (Eastern Alps). J. Petrol. 58, 1451–1472.
Ionov, D.A., Seitz, H.M., 2008. Lithium abundances and isotopic compositions in mantle xenoliths from subduction and intra-plate settings: mantle sources vs. eruption histories. Earth Planet. Sci. Lett. 266, 316–331.
Jégo, S., Dasgupta, R., 2013. Fluid-present melting of sulfide-bearing ocean-crust: experimental constraints on the transport of sulfur from subducting slab to mantle wedge. Geochim. Cosmochim. Acta 110, 106–134.
Kelemen, P.B., Manning, C.E., 2015. Reevaluating carbon fluxes in subduction zones, what goes down, mostly comes up. Proc. Natl. Acad. Sci. U.S.A. 112, E3997–E4006.
Klein, F., Grozeva, N.G., Seewald, J.S., 2019. Abiotic methane synthesis and serpentinization in olivine-hosted fluid inclusions. Proceed. Natl. Acad. Sci. 116, 17666–17672.
Malaspina, N., Poli, S., Fumagalli, P., 2009. The oxidation state of metasomatized mantle wedge: insights from C–O–H-bearing garnet peridotite. J. Petrol. 50, 1533–1552.
Malaspina, N., Tumiati, S., 2012. The role of C-O-H and oxygen fugacity in subduction-zone garnet peridotites. Eur. J. Mineral. 24, 607–618.
Marocchi, M., Mair, V., Tropper, P., Bargossi, G.M., 2009. Metasomatic reaction bands at the Mt. Hochwart gneiss-peridotite contact (Ulten Zone, Italy): insights into fluid-rock interaction in subduction zones. Mineral. Petrol. 95, 251–272.
Martin, S., Godard, G., Prosser, G., Schiavo, A., Bernoulli, D., Ranalli, G., 1998. Evolution of the deep crust at the junction Austroalpine/Southalpine; the Tonale Nappe. Memorie di Scienze Geologiche 3–50.
Martin, S., Montresor, L., Mair, V., Pellegrini, G.B., Avanzini, M., Fellini, G., Gambillara, R., Tumiati, S., Santuliana, E., Monopoli, B., Gaspari, D., Sapigni, M., Surian, N., 2009. Foglio 025 Rabbi. In: ISPRA, S.G.d.I. (Ed.), Note Illustrative della Carta Geologica D'italia Alla Scala, p. 192, 1:50.000.
Masci, L., Dubacq, B., Verlaguet, A., Chopin, C., Andrade, V.D., Herviou, C., 2019. A XANES and EPMA study of Fe3+ in chlorite: importance of oxychlorite and implications for cation site distribution and thermobarometry. Am. Mineralog. 104, 403–417.
Matjuschkin, V., Blundy, J.D., Brooker, R.A., 2016. The effect of pressure on sulphur speciation in mid- to deep-crustal arc magmas and implications for the formation of porphyry copper deposits. Contribut. Mineral. Petrol. 171, 66.
Mattey, D., Lowry, D., Macpherson, C., 1994. Oxygen-isotope composition of mantle peridotite. Earth Planet. Sci. Lett. 128, 231–241.
McDonough, W.F., Sun, S.-s., 1995. The composition of the earth: chemical evolution of the mantle. Chem. Geol. 120, 223–253.
Nimis, P., Morten, L., 2000. P-T evolution of 'crustal' garnet peridotites and included pyroxenites from Nonsberg area (upper Austroalpine), NE Italy: from the wedge to the slab. J. Geodyn. 30, 93–115.
O'Neill, H.S.C., 2021. The thermodynamic controls on sulfide saturation in silicate melts with application to ocean floor basalts. Magma Redox Geochem. 177–213.
O'Neill, H.S.C., McCammon, C.A., Canil, D., Rubie, D.C., Ross, C.R., Seifert, F., 1993. Mössbauer spectroscopy of mantle transition zone phases and determination of minimum Fe3+ content. Am. Mineralog. 78, 456–460.
Peslier, A.H., 2010. A review of water contents of nominally anhydrous natural minerals in the mantles of Earth, Mars and the Moon. J. Volcanol. Geotherm. Res. 197, 239–258.
Rampone, E., Morten, L., 2001. Records of crustal metasomatism in the garnet peridotites of the Ulten Zone (Upper Austroalpine, Eastern Alps). J. Petrol. 42, 207–219.
Ranalli, G., Martin, S., Mahatsente, R., 2005. Continental subduction and exhumation: an example from the Ulten Unit. In: Tonale Nappe, Eastern Austroalpine. Geological Society, 243. Special Publications, London, pp. 159–174.
Rielli, A., Tomkins, A.G., Nebel, O., Brugger, J., Etschmann, B., Paterson, D., 2018. Garnet peridotites reveal spatial and temporal changes in the oxidation potential of subduction. Sci. Rep. 8.
Rielli, A., Tomkins, A.G., Nebel, O., Brugger, J., Etschmann, B., Zhong, R., Yaxley, G.M., Paterson, D., 2017. Evidence of sub-arc mantle oxidation by sulphur and carbon. Geochem. Perspect. Lett. 3, 124–132.
Sapienza, G.T., Scambelluri, M., Braga, R., 2009. Dolomite-bearing orogenic garnet peridotites witness fluid-mediated carbon recycling in a mantle wedge (Ulten Zone, Eastern Alps, Italy). Contribut. Mineral. Petrol. 158, 401–420.
Scambelluri, M., Bebout, G.E., Belmonte, D., Gilio, M., Campomenosi, N., Collins, N., Crispini, L., 2016. Carbonation of subduction-zone serpentinite (high-pressure ophicarbonate; Ligurian Western Alps) and implications for the deep carbon cycling. Earth Planet. Sci. Lett. 441, 155–166.
Scambelluri, M., Hermann, J., Morten, L., Rampone, E., 2006. Melt-versus fluid-induced metasomatism in spinel to garnet wedge peridotites (Ulten Zone, Eastern Italian Alps): clues from trace element and Li abundances. Contribut. Mineral. Petrol. 151, 372–394.
Schwarzenbach, E.M., Gill, B.C., Gazel, E., Madrigal, P., 2016. Sulfur and carbon geochemistry of the Santa Elena peridotites: comparing oceanic and continental processes during peridotite alteration. Lithos 252-253, 92–108.
Shcheka, S.S., Wiedenbeck, M., Frost, D.J., Keppler, H., 2006. Carbon solubility in mantle minerals. Earth Planet. Sci. Lett. 245, 730–742.
Shirey, S.B., Cartigny, P., Frost, D.J., Keshav, S., Nestola, F., Nimis, P., Pearson, D.G., Sobolev, N.V., Walter, M.J., 2013. Diamonds and the geology of mantle carbon. Carbon Earth 75, 355–421.
Sossi, P.A., Burnham, A.D., Badro, J., Lanzirotti, A., Newville, M., O'Neill, H.S.C., 2020. Redox state of Earth's magma ocean and its Venus-like early atmosphere. Sci. Adv. 6, eabd1387.
Stagno, V., Cerantola, V., Aulbach, S., Lobanov, S., McCammon, C.A., Merlini, M., 2019. Carbon bearing phases throughout Earth - evolution through space and time. In: Orcutt, B.N., Danielle, I., Dasgupta, R. (Eds.), Deep Carbon: Past to Present. Cambridge University Press, pp. 66–88.
Tumiati, S., Fumagalli, P., Tiraboschi, C., Poli, S., 2013. An experimental study on COH-bearing peridotite up to 3·2 GPa and implications for crust–mantle recycling. J. Petrol. 54, 453–479.
Tumiati, S., Godard, G., Martin, S., Klotzli, U., Monticelli, D., 2007. Fluid-controlled crustal metasomatism within a high-pressure subducted melange (Mt. Hochwart, Eastern Italian Alps). Lithos 94, 148–167.
Tumiati, S., Malaspina, N., 2019. Redox processes and the role of carbon-bearing volatiles from the slab-mantle interface to the mantle wedge. J. Geol. Soc. Lond. 176, 388–397.
Tumiati, S., Recchia, S., Remusat, L., Tiraboschi, C., Sverjensky, D.A., Manning, C.E., Vitale Brovarone, A., Boutier, A., Spanu, D., Poli, S., 2022. Subducted organic matter buffered by marine carbonate rules the carbon isotopic signature of arc emissions. Nat. Commun. 13, 2909.
Tumiati, S., Thoni, M., Nimis, P., Martin, S., Mair, V., 2003. Mantle-crust interactions during Variscan subduction in the Eastern Alps (Nonsberg-Ulten zone): geochronology and new petrological constraints. Earth Planet. Sci. Lett. 210, 509–526.
Wang, X., Wang, Z., Zhang, W., Ma, L., Chen, W., Cai, Y.-C., Foley, S., Wang, C.Y., Li, J., Deng, J., Feng, Y., Zong, K., Hu, Z., Liu, Y., 2024. Sulfur isotopes of lamprophyres and implications for the control of metasomatized lithospheric mantle on the giant Jiaodong gold deposits, eastern China. GSA Bulletin.
Whitney, D.L., Evans, B.W., 2010. Abbreviations for names of rock-forming minerals. Am. Mineralog. 95, 185–187.
Wykes, J.L., Newton, R.C., Manning, C.E., 2008. Solubility of andradite, $Ca_3Fe_2Si_3O_{12}$, in a 10 mol% NaCl solution at 800 °C and 10 kbar: implications for the metasomatic origin of grandite garnet in calc-silicate granulites. Am. Mineralog. 93, 886–892.
Wyllie, P.J., Huang, W.L., Otto, J., Byrnes, A.P., 1983. Carbonation of peridotites and decarbonation of siliceous dolomites represented in the system CaO-MgO-SiO_2-CO_2 to 30 kbar. Tectonophysics 100, 359–388.
Zheng, Y.-F., Chen, Y.-X., 2016. Continental versus oceanic subduction zones. Natl. Sci. Rev. 3, 495–519.